Atmos. Chem. Phys. Discuss., 12, 7073–7123, 2012
www.atmos-chem-phys-discuss.net/12/7073/2012/
doi:10.5194/acpd-12-7073-2012

Atmospheric Chemistry and Physics Discussions

Aerosol indirect effects from shipping emissions: sensitivity studies with the global aerosol-climate model ECHAM-HAM

K. Peters[1,2,*], **P. Stier**[3], **J. Quaas**[4], **and H. Graßl**[1]

[1]Max Planck Institute for Meteorology, Hamburg, Germany
[2]International Max Planck Research School on Earth System Modelling, Hamburg, Germany
[3]Department of Physics, University of Oxford, UK
[4]Institute for Meteorology, University of Leipzig, Leipzig, Germany
[*]now at: Monash University, School of Mathematical Sciences, Clayton, VIC 3800, Australia

Received: 23 February 2012 – Accepted: 24 February 2012 – Published: 8 March 2012

Correspondence to: K. Peters (karsten.peters@monash.edu)

Published by Copernicus Publications on behalf of the European Geosciences Union.

Abstract

In this study, we employ the global aerosol-climate model ECHAM-HAM to globally assess aerosol indirect effects (AIEs) resulting from shipping emissions of aerosols and aerosol precursor gases. We implement shipping emissions of sulphur dioxide (SO_2), black carbon (BC) and particulate organic matter (POM) for the year 2000 into the model and quantify the model's sensitivity towards uncertainties associated with the emission parameterisation as well as with the shipping emissions themselves. Sensitivity experiments are designed to investigate (i) the uncertainty in the size distribution of emitted particles, (ii) the uncertainty associated with the total amount of emissions, and (iii) the impact of reducing carbonaceous emissions from ships.

We use the results from one sensitivity experiment for a detailed discussion of shipping-induced changes in the global aerosol system as well as the resulting impact on cloud properties. From all sensitivity experiments, we find AIEs from shipping emissions to range from $-0.07 \pm 0.01\,\mathrm{W\,m^{-2}}$ to $-0.32 \pm 0.01\,\mathrm{W\,m^{-2}}$ (global mean value and inter-annual variability as a standard deviation). The magnitude of the AIEs depends much more on the assumed emission size distribution and subsequent aerosol microphysical interactions than on the magnitude of the emissions themselves. It is important to note that although the strongest estimate of AIEs from shipping emissions in this study is relatively large, still much larger estimates have been reported in the literature before on the basis of modelling studies. We find that omitting just carbonaceous particle emissions from ships favours new particle formation in the boundary layer. These newly formed particles contribute just about as much to the CCN budget as the carbonaceous particles would, leaving the globally averaged AIEs nearly unaltered compared to a simulation including carbonaceous particle emissions from ships.

ACPD
12, 7073–7123, 2012

1 Introduction

Ship tracks are widely seen as one of the most prominent manifestations of anthropogenic aerosol indirect effects (AIEs), or the change in cloud properties by anthropogenic aerosols serving as cloud condensation nuclei. A very uncertain and scientifically interesting question, however, is about the climatically relevant large-scale forcing by AIEs due to ship emissions.

In the past decades, a whole suite of AIE-hypotheses has been put forward of which the "Twomey-effect", or first AIE, is the most prominent. For this effect, an increase in available cloud condensation nuclei (CCN) eventually leads to more and smaller cloud droplets if the liquid water content of the respective cloud remains constant. More cloud droplets increase the total droplet surface area by which the cloud albedo is enhanced; an effect which was put into the general context of anthropogenic pollution by Twomey (1974). Other AIE-hypotheses include effects on cloud lifetime (Albrecht, 1989; Small et al., 2009) or cloud top height (Koren et al., 2005; Devasthale et al., 2005). Especially the latter hypotheses are far from being verified (e.g., Stevens and Feingold, 2009). In total, AIEs are subject to the largest uncertainties of all radiative forcing (RF) components of the Earth System, when it comes to assessing human induced climate change (Forster et al., 2007). However, there exists broad consensus that on global average, AIEs have a cooling effect on the Earth System with the most recent multi-model estimate being $-0.7 \pm 0.5\,\mathrm{W\,m^{-2}}$ (Quaas et al., 2009).

Aerosols and aerosol precursor gases also lead to aerosol direct radiative effects (DREs), i.e. the aerosol particles absorb and scatter the incident solar radiation directly (Ångström, 1962). While regionally, a warming effect by aerosol absorption can be substantial (e.g., Peters et al., 2011a), globally, aerosol-DREs are believed to exert a net radiative cooling of about $-0.3 \pm 0.2\,\mathrm{W\,m^{-2}}$ on the Earth System (Myhre, 2009). In the recent climate-change discussion, the mitigation of carbonaceous emissions has attracted substantial attention in the scientific community. BC aerosols are associated with a net positive radiative forcing (RF) at the top-of-atmosphere (TOA) due to their strong absorption of incident solar radiation, also leading to semi-direct effects on cloud

ACPD
12, 7073–7123, 2012

cover (Koch and Del Genio, 2010). Thus, BC is perhaps the third largest contributor to positive RF, following CO_2 and methane, and reducing its emission could contribute to delaying global warming due to anthropogenic climate change (e.g., Bond, 2007). However, this neglects the ability of BC particles to act as cloud condensation nuclei (CCNs) when they internally mix with hygroscopic species through microphysical and chemical ageing. This possibly leads to an overestimation of the cooling potential of BC mitigation options (e.g., Pierce et al., 2007; Spracklen et al., 2011).

Shipping is the most cost-effective mean of long distance cargo transportation (e.g., Borken-Kleefeld et al., 2010) and global ship traffic is expected to increase due to increasing international trade (e.g., Eyring et al., 2005a). Because greenhouse gas emissions from seagoing ships are not included in the Kyoto Protocol (1997), seagoing ships are one of the least regulated sources of anthropogenic emissions. It is estimated that in 2007, seagoing ships had a share of 2.7 % in all anthropogenic CO_2 emissions (Buhaug et al., 2009). Other gaseous emissions from ships include large amounts of nitrious oxides (NO_x), methane and non-methane hydrocarbons. Furthermore, combustion of low-quality fuel, as used in ship engines, produces large amounts of aerosols and aerosol precursors. These come in form of particulate matter consisting of elemental (black) and organic carbon, ash and particles forming from sulfuric acid (e.g., Eyring et al., 2005b; Petzold et al., 2008). These constituents, being emitted in mostly pristine marine environments, can serve as cloud condensation nuclei (CCN) (e.g., Petzold et al., 2008) and result in AIEs.

AIEs from shipping emissions are occasionally manifested in linear cloud structures referred to as “ship tracks”. These form as a result from ship effluents providing additional CCN which can potentially alter the micro- and macrophysical properties of maritime liquid-water clouds. Ship-tracks have been characterised in detail by a number of studies (see Peters et al., 2011b, and references therein). Those studies all focus on the detection and characterisation of ship tracks on local scales. The globally averaged RF of just ship tracks has been estimated to range from −0.4 to −0.6 mW m^{-2} (Schreier et al., 2007).

ACPD
12, 7073–7123, 2012

From a climate point of view however, it is important to get an impression of the large-scale RF resulting from shipping emissions. Apart from leading to ship-tracks, shipping emissions also have the potential to change the micro- and macrophysical properties of cloud fields also at a large, climatically relevant, scale. This is especially true for areas with widespread shipping emissions such as in the Northern Atlantic and Pacific Oceans. Two observational studies have so far attempted to quantify such large scale effects from shipping emissions. While Devasthale et al. (2006) found evidence of cloud-property modification from shipping emissions over European coastal waters, Peters et al. (2011b) could not identify significant changes of cloud properties downwind of shipping routes over tropical oceans.

The above studies nicely illustrate the difficulty of establishing sound cause-and-effect relationships from observations. However, atmospheric modelling allows to explicitly separate the impact of shipping from the natural background. In recent years, modelling the impact of shipping emissions on the Earth System on climate relevant scales has received increasing attention. Most of these modelling studies focus on changes related to atmospheric chemistry and composition (Eyring et al., 2007, and references therein) and assessing global AIEs from shipping emissions has to date just been performed with two distinct models.

Capaldo et al. (1999) used shipping emissions of sulphur and organic material as presented in Corbett et al. (1999) in a global chemical transport model. The derived changes in atmospheric composition were then used to perform offline calculations of changes in CCN and the resulting RF. Their sensitivity tests, performed by varying input parameters like the background CCN concentration or the CCN cut-off radius, revealed RF values ranging from -0.06 to $-0.21\,\mathrm{W\,m^{-2}}$. Lauer et al. (2007) used three different shipping emission inventories and estimated globally averaged AIEs to range from -0.19 to $-0.6\,\mathrm{W\,m^{-2}}$ and Lauer et al. (2009) tested the impact of future regulations regarding the sulfur content of marine bunker fuel (IMO, 1998) and found reduced AIEs despite increasing fuel consumption. The DRE resulting from shipping emissions is small and estimated to range from -47.5 to $-9.1\,\mathrm{mW\,m^{-2}}$ (Balkanski et al.,

ACPD
12, 7073–7123, 2012

2010; Eyring et al., 2010).

As the present estimate of the total greenhouse gas (GHG) RF, as given by the IPCC, is about $+3\,W\,m^{-2}$, the above mentioned model results suggest that AIEs and DREs from shipping might mask a significant portion of the GHG induced radiative forcing. This masking may be reduced due to shipping emission regulations (e.g., Lauer et al., 2009), but even without those policy regulations, the estimated current cooling effect of shipping emissions will switch to a long-term warming (e.g., Fuglestvedt et al., 2009). This is because the warming related to the ship-emitted CO_2 acts on timescales on the order of centuries whereas the cooling of the sulphuric compounds acts on timescales of decades when taking changes in oceanic heat content into account. Furthermore, evidence suggests that combustion of cleaner ship fuel also leads to reduced emission of particulate BC (Lack and Corbett, 2012), also reducing its potential cooling effect.

In this study, we employ the state of the art global aerosol-climate model ECHAM-HAM to provide (1) insight into ship-emission processing in the model, and (2) a range of estimates of AIEs from shipping emissions. We derive this range of estimates from a series of sensitivity experiments which are designed to investigate (i) the uncertainties related to the size distribution of emitted particles, (ii) the uncertainty associated with the total amount of emissions, and (iii) the impact of reducing carbonaceous emissions from ships. The model framework, the used shipping emissions inventory and the experimental setup are described in Sect. 2. A detailed view of ship-emission processing in ECHAM-HAM is given in Sect. 3 and the results of the sensitivity experiments are presented in Sect. 4. Summary and conclusions are given in Sect. 5.

2 Model and experiment setup

Here, we utilise the global aerosol-climate model ECHAM-HAM (Zhang et al., 2012) to thoroughly investigate the effect of shipping emissions on clouds. In the simulations discussed here, cloud cover is computed following a relative humidity-based approach (Sundqvist et al., 1989) and the treatment of convective clouds and -transport is based

ACPD
12, 7073–7123, 2012

on the mass-flux scheme of Tiedtke (1989). Cloud microphysics are computed according to Lohmann et al. (2007) some details of which are described below. Transport of physical quantities in gridpoint-space, such as water vapour, cloud water and -ice, and trace components is performed via a semi-lagrangian transport scheme (Lin and Rood, 1996). Here, ECHAM-HAM is used in nudged mode to relax the prognostic variables (vorticity, divergence, temperature and surface pressure) towards an atmospheric reference state (ERA-Interim reanalysis data; Simmons et al., 2007).

2.1 Aerosol treatment

ECHAM is coupled to HAM, a microphysical aerosol module which calculates the evolution of an aerosol population represented by seven interacting internally and externally mixed log-normal aerosol modes (Zhang et al., 2012). In the setup applied here, HAM treats sulfate (SU), black carbon (BC), particulate organic matter (POM), sea salt (SS) and dust (DU) aerosol. The modes consist of compounds with either low or no solubility (insoluble modes) or an internal mixture of insoluble and soluble compounds (soluble modes). The microphysical interaction among the modes, such as coagulation, condensation of sulfuric acid on the aerosol surface, and water uptake are calculated by the microphysical core M7 (Vignati et al., 2004). New particle formation is calculated as in the experiments of Kazil et al. (2010): particle formation via (1) cluster activation and (2) neutral- and charged activation are treated following Kulmala et al. (2006) and Kazil and Lovejoy (2007), respectively. Further, HAM treats emissions, sulfur chemistry (Feichter et al., 1996), dry and wet deposition and sedimentation and is coupled to radiative processes.

2.2 Cloud microphysics

Here, cloud microphysical properties are derived using a double-moment scheme which solves prognostic equations for cloud water and -ice mass mixing ratios as well as for the number of cloud droplets and -ice crystals Lohmann et al. (2007). The

ACPD
12, 7073–7123, 2012

parametrised microphysical processes relevant for liquid-water cloud properties are nucleation of cloud droplets, condensational growth of cloud droplets, autoconversion of cloud droplets to form rain water, accretion of cloud droplets by snow and by rain, and melting of cloud ice and snow. The amount of cloud liquid water mixing ratio, q_l, inside a grid box is provided by the condensation scheme (Sundqvist et al., 1989) with an additional source from convective detrainment, and is a prerequisite for performing the calculations of cloud microphysics.

The cloud microphysical scheme is coupled to HAM so that changes in the aerosol- and cloud population can feed back onto each other. Cloud droplet nucleation is parametrised as an empirical function of aerosol number concentrations (Lohmann et al., 2007) and Köhler theory based CCN diagnostics are also included (Stier et al., 2012). Autoconversion, i.e. conversion from cloud droplets to form precipitation, is treated according to Khairoutdinov and Kogan (2000).

In ECHAM, the convection parametrisation provides for vertical transport and horizontal detrainment of cloud water and CCN. The detrained CCN then serve as potential nuclei for stratiform clouds which form at the detrainment level. Convective clouds therefore only have an indirect effect on radiation through detrainment of liquid water to the stratiform scheme, i.e. they are assigned a cloud cover of zero.

2.3 Aerosol-emission setup

The emissions of dust (Tegen et al., 2002), sea salt (Guelle et al., 2001) and dimethyl sulfide (DMS, Kettle and Andreae, 2000) are computed on-line. The emissions of carbonaceous and sulfuric compounds, except those from shipping, are prescribed according to the AeroCom (Kinne et al., 2006) recommendations (for the year 2000 Dentener et al., 2006). Gaseous species (e.g., OH, NO_x, ozone) are prescribed as monthly values after Horowitz et al. (2003).

We substitute the AeroCom shipping emissions (EDGAR Bond et al., 2004; Olivier et al., 2005) with a dataset produced within the European Integrated Project QUANTIFY (EU-IP QUANTIFY) which comprises globally gridded data of shipping emissions

ACPD
12, 7073–7123, 2012

for the year 2000 (Behrens, 2006). This inventory offers a consistent geographical distribution for all emitted components and we compare its total annual emissions and geographical distribution of SO_2 emissions to those of the standard AeroCom inventory in Table 1 and Fig. 1; the geographical distribution of carbonaceous emissions is similar among both datasets.

In the QUANTIFY inventory, the geographical distribution of shipping emissions is performed by using a combination of COADS (Comprehensive Atmosphere-Ocean Data Set) and AMVER (Automatic Mutual-Assistance Vessel Rescue System) ship-traffic densities for the years 2000 and 2001/2002, respectively. To distribute the annual emissions in the QUANTIFY inventory, about 1 000 000 marine reports were used as input in both the COADS and AMVER datasets for deriving global ship reporting frequencies as illustrated in Endresen et al. (2003). The global distributions are shown in Dalsøren et al. (2009).

In addition to the uncertainties related to the geographical distribution of the shipping emissions, there also exist inherent uncertainties in the total fuel consumption of seagoing ships. In the QUANTIFY inventory, the total annual fuel consumption is estimated at 172.5 Mt of total fuel consumption for the year 2000 which is substantially lower than the estimates of Corbett and Koehler (2003) and Eyring et al. (2005b), being 289 Mt and 280 Mt, respectively. The large differences between QUANTIFY and the other inventories concerning the fuel consumption estimates have been a matter of intense debate and it has been shown that the assumed level of activity (or "days at sea") is the main reason for the large differences (e.g., Endresen et al., 2004; Corbett and Koehler, 2004).

We apply the emissions as a constant flux (in $kg\,m^{-2}\,s^{-1}$) of annually averaged data to the model layer above the surface layer. Monthly resolved ship traffic density datasets do exist (e.g., Wang et al., 2007), but the uncertainty introduced by using annually mean emission fields is probably negligible compared to the uncertainty associated with the emissions themselves (A. Lauer, personal communication, 2011).

ACPD
12, 7073–7123, 2012

2.4 Experimental setup

To quantify the effect of shipping emissions on clouds, we perform and analyse a total of seven GCM experiments. The experiments are designed to highlight the uncertainties associated with the total global annual fuel consumption and the emission size distribution as well as to investigate the potential and implications of mitigating carbonaceous-particle emissions from ships. Simulations are performed with a horizontal resolution of T63 (about $1.8^{\circ} \times 1.8^{\circ}$) and a vertical resolution of 31 levels up to 10 hPa. Monthly mean sea surface temperatures and sea ice cover are prescribed according to the AMIP II dataset (Atmospheric Model Intercomparison Project; Taylor et al., 2000). The performed simulations span the time period from October 1999 to December 2004. The first three months are considered as model spin-up and the analysis is then performed on the remaining five years.

In experiment *A*, we run the model with the QUANTIFY inventory using the originally implemented shipping emissions parametrisation (AeroCom, "old" in Table 2). We slightly modify the original emission parametrisation because we found it to be inconsistent – the carbonaceous compounds from shipping emissions were originally assigned to the model's surface layer whereas the sulphuric compounds where assigned to one layer above the model's surface layer. This is because shipping emissions are considered as part of industrial emissions in AeroCom. For industrial emissions of sulphuric compounds, an emission height well above the surface is assumed because industrial plants emit most of their exhausts from smoke stacks. This method is not applied to industrial carbonaceous emissions because their fraction in the stack-emissions is assumed to be negligible (S. Kinne, personal communication, 2010). We therefore modify the emission routine in HAM so that all emissions from ships are consistently assigned to the model layer above the surface layer.

In experiment *A*, the emissions of BC and POM are assigned to the insoluble Aitken mode with a number mean radius of $\bar{r} = 0.03\,\mu\text{m}$ and a standard deviation of the log-normal distribution of $\sigma = 1.59$. The bulk of sulfuric emissions is emitted in form of

ACPD
12, 7073–7123, 2012

gaseous SO_2. Fast processing of gaseous SO_2 emissions is accounted for by allowing a certain fraction f_{SO_4} of the emitted sulfuric mass to transform to particulate sulfate at the point of emission instantaneously (i.e., within one timestep). In the AeroCom setup as used in experiment *A*, $f_{SO_4} = 2.5\,\%$. Of this particulate sulfate, 50 % is assigned to the soluble Accumulation mode (AS, $\bar{r} = 0.075\,\mu m$, $\sigma = 1.59$) and 50 % is assigned to the soluble Coarse mode (CS, $\bar{r} = 0.75\,\mu m$, $\sigma = 2$).

To investigate the uncertainty associated with the insufficient knowledge of the emission size distribution, we developed experiment *B*. A close look at the original emission parametrisation as used in *A* yields significant discrepancies to what is currently known about the microphysical and chemical properties of shipping emissions.

First, recent studies indicate that the f_{SO_4} is often larger than 2.5 %. Agrawal et al. (2008) find a value of $f_{SO_4} = 3.7$–5 % for a fuel sulphur content of 2.05 %. Lack et al. (2009) deduce $f_{SO_4} = 1.4\,\% \pm 1.1\,\%$ and $f_{SO_4} = 3.9\,\% \pm 2.0\,\%$ for low (< 0.5 %) and high (> 0.5 %) fuel sulphur content, respectively. Therefore, we increase f_{SO_4} from 2.5 to 4.5 % in experiment *B*, considering the fact that the globally weighted marine fuel sulphur content is estimated at 2.68 % for 2002 (Endresen et al., 2004).

Second, the assumed emission size distribution of primary sulfate particles may be too large in AeroCom (see above). A number of studies have shown that ships emit a suite of particles which are all in the size range $\bar{r} < 0.05\,\mu m$. Specifically, Petzold et al. (2008) investigated the particle size distribution in an aged plume (20 min old, which is roughly on the order of the model timestep) of shipping emissions over the English Channel and found that the modal radius of the ship-emitted particles was ≈ 0.02–$0.04\,\mu m$. Because this size range corresponds to that of the Aitken mode in HAM, we assign all ship-emitted primary sulfate particles to the soluble Aitken mode (modal radius: 0.03 µm) in experiment *B*.

Third, all carbonaceous particles from shipping emissions are assumed insoluble at the point of emission in the original AeroCom parametrisation. This assumption however is inconsistent with recent laboratory measurements. Kireeva et al. (2010) showed that freshly emitted soot from a ship engine burning fuel with a sulfur content

ACPD
12, 7073–7123, 2012

of just 0.5 % yields significantly higher solubility than soot emitted from an aircraft- or truck engine. Motivated by these results, we assign all ship-emitted carbonaceous particles to the soluble Aitken mode (modal radius: 0.03 µm) in experiment *B*, similar to Lauer et al. (2007). Therefore, the model setup for experiment *B* also yields a better comparison framework to earlier studies.

In the experiments *Asc* and *Bsc*, we scale the emissions of the QUANTIFY inventory in order to investigate the uncertainty associated with the unknown total annual fuel consumption from ships. As previously noted, the QUANTIFY inventory represents a lower estimate among the currently used shipping emission inventories. Therefore, the mass of annually emitted particulate- and gaseous species is scaled to values which meet the ones published by Corbett and Koehler (2003). There, the annual total emission of SO_2 is given as 12.98 Tg (based on ship activity for the year 2001). Relating this to the given value in the QUANTIFY inventory (7.95 Tg; year 2000), we scale the emissions of SO_2, BC and POM by a factor of 1.63 for use in the experiments *Asc* and *Bsc*.

In the experiments *BnoBC* and *BnoC*, we explore the potential effects of mitigating the emission of carbonaceous compounds from ships. For both experiments, we employ the model with the newly introduced emission parametrisation (see experiment *B*). We omit all BC and all carbonaceous emissions from ships in experiments *BnoBC* and *BnoC*, respectively. These simulations thus represent idealised sensitivity studies because no potential side-effects that BC mitigation may have on the magnitude of sulfuric emissions (and vice-versa Lack and Corbett, 2012, and references therein) are included.

3 Ship-emission induced aerosol processes in ECHAM-HAM

To illustrate the pathway from shipping emissions to changes in the TOA radiation budget as modelled by ECHAM-HAM, we perform a stepwise analysis using the results obtained from experiment *B*. The steps in this analysis consider the changes in

ACPD
12, 7073–7123, 2012

- emissions
- aerosol mass- and number burdens
- CCN concentrations
- cloud macro- and microphysical properties
- radiation budget.

In the following, the displayed figures represent simulated five-year mean values. Statistical significance is computed by applying a two-tailed Student's t-test to the respective five annually averaged fields and the standard deviation of the five annual means in each grid-box.

3.1 Changes in emissions and mass burdens

The global distributions of total sulphur (comprised of sulphur dioxide (SO_2), sulfate and dimethyl sulphide (DMS)), black carbon (BC) and particulate organic matter (POM) emissions as used in experiment *B* are shown in Fig. 2. Shipping emissions represent just a small fraction of the global mean anthropogenic emissions: 7.2 % for S, 0.5 % of BC and 0.25 % of POM. However, emissions from shipping often occur in otherwise pristine marine environments and can therefore result in substantial modifications of the aerosol populations in the marine boundary layer.

As shown in Fig. 3, the relative changes in SO_2 column burden are very similar to the spatial pattern of shipping emissions on global oceans. We obtain the largest changes over the Northern Hemisphere (NH) Atlantic Ocean, the Northern Indian Ocean and the Northern Pacific Ocean, with most changes being statistically significant at the 90 % level. Relative changes in sulfate column burden show smaller values in Southeast Asia compared to the Western European coast although the changes in SO_2 column burden are of similar magnitudes. Because SO_2 is oxidised to H_2SO_4 by OH, this can

ACPD
12, 7073–7123, 2012

be explained by higher OH abundance over the North Atlantic in the monthly prescribed fields (Horowitz et al., 2003).

The relative changes in atmospheric BC and OC burdens only show distinct patterns over the Northwestern Atlantic and none of these features is statistically significant at the 90 % level – a surprising result as shipping emissions represent the only source of these species over oceans. Therefore, it is plausible that the emissions of sulfuric constituents from ships are the ones which ultimately determine the total effect on both cloudy- and clear sky radiation.

3.2 Changes in aerosol number

It is feasible to track the models' response induced by a certain change in emission parameters through each aerosol mode, thereby clarifying the underlying processes leading to the observed total response. We order the analysis from the smallest to largest aerosol modes. We show the vertically- and meridionally resolved changes in particle number concentrations in Fig. 4.

Due to the increased availability of condensable material, i.e. sulphuric acid (H_2SO_4), non-soluble particles are converted to soluble ones via condensation of H_2SO_4 onto them. This can clearly be depicted for the insoluble Aitken (KI), Accumulation (AI) and Coarse (CI) modes (top row Fig. 4).

The population of soluble Nucleation mode (NS) particles by design consists only of secondary aerosol resulting from new particle formation, mainly nucleated from sulfuric acid (H_2SO_4). Vertically resolved, pronounced relative increases in NS-particle concentrations are constrained to the NH mid- and upper troposphere (Kazil et al., 2010) as well as some parts of tropical boundary layer (bottom row Fig. 4). Because these areas are relatively unpolluted, the lack of condensational sinks favours particle nucleation. However, a decrease in NS-particle numbers is obtained for the NH mid-latitude boundary layer and lower troposphere (up to ≈ 800 hPa). There, condensation of H_2SO_4 onto pre-existing particles substantially dominates over new particle formation.

ACPD
12, 7073–7123, 2012

Soluble Aitken mode (KS) particle number concentrations decrease in the NH boundary layer (bottom row Fig. 4). The cause for this is two-fold. Firstly, less nucleated NS-particles (see above) result in less particles growing to KS and secondly, the increase of emitted primary KS-particles leads to increased condensation of H_2SO_4 onto them. This yields faster growth rates to the soluble Accumulation mode (AS) and thus shorter residence time in KS. For the mid- and upper troposphere, the overall increase in KS-particle number concentrations results from growth of the increasingly present NS-particles (see above).

Particle number burdens in the soluble Accumulation mode (AS) increase everywhere on the globe. In relative terms, regions of largest increase correspond to those of highest shipping emissions in the North Atlantic, North Pacific, mid-Indian Ocean, and Southeast Asia (not shown). The vertically and meridionally resolved changes in AS-particle number concentrations show an increase practically everywhere throughout the troposphere (bottom row Fig. 4). Especially in the NH boundary layer, the condensational growth of the emitted KS-particles thus leads to a significant increase ("accumulation") of particles in AS. This is of particular interest as that size range is most suitable for CCN-activation at supersaturations typical for stratocumulus clouds (80–100 nm at 0.2 % supersaturation, e.g., Pierce and Adams, 2009).

The increase in soluble Coarse mode (CS) particle concentrations is confined to the lower troposphere, but is not as large as for AS and is not statistically significant at any point in the troposphere.

To summarise, the introduction of shipping emissions leads to reduced particle nucleation and substantially increased condensational growth rates of primary Aitken-mode sized particles in the NH boundary layer. This results in decreased particle number concentrations in both NS and KS and increased AS-particle number concentrations in the NH boundary layer. Furthermore, the increased availability of sulfuric compounds leads to increased particle nucleation rates throughout the tropical troposphere, which results in increased particle number concentrations in all soluble modes but the Coarse mode.

ACPD
12, 7073–7123, 2012

The aforementioned faster growth rates of aerosol particles could in fact lead to a reduction of their atmospheric lifetimes due to enhanced wet- and dry deposition. Aerosol lifetimes, defined here as the ratio of burdens over sources, are displayed in Table 3. Indeed, lifetimes are slightly reduced for all aerosol types in experiment *B*, with the exception of sea salt.

The impact of the shipping emissions on the aerosol population and its direct effect on atmospheric radiation is illustrated by the relative changes in AOD and its fine mode (i.e. the contribution from particles smaller than 1 µm in diameter), as shown in Fig. 5. Statistically significant increases in both the AOD and its fine mode are obtained for most of the Western European coastal waters as well as some areas off the western coast of North America. The globally averaged relative increase in the fine-mode AOD is larger than that obtained for the total AOD. This should be expected, as the main increase in particle numbers is found for Accumulation mode sized particles, which are by definition smaller than 1 µm in diameter. The impact of this change in AOD on clear-sky atmospheric radiation will be discussed in Sect. 3.5.

3.3 Changes in predicted CCN concentrations

We show vertically- and meridionally resolved changes in CCN concentrations, derived from Köhler theory, at various supersaturations in Fig. 6. At low supersaturations (0.04 %), large areas in the NH lower- to mid troposphere exhibit a significant increase in CCN concentrations, with values > 10 % occurring in the boundary layer north of 60° N, closely following the changes in AS particle number. CCN concentrations at higher supersaturations show a similar pattern but an increasing contribution of KS number changes, in particular in the tropics. This again hints at aerosol processing in the boundary layer – smaller particles (higher supersaturations) are found near the emission sources whereas larger particles (smaller supersaturations) are found higher up in the troposphere as a result of microphysical- and chemical ageing during transport. Distinct and often statistically significant increases in CCN concentrations are also found for the mid to high tropical troposphere.

ACPD
12, 7073–7123, 2012

Summarising, it is evident that shipping emissions lead to an increased number of CCNs at supersaturations typical for marine liquid water clouds. This follows from distinct increases in AS particle numbers, especially in the NH boundary layer, as a result from increased particle growth rates (see Sect. 3.2).

3.4 Changes in cloud micro- and macrophysical properties

As shown in Fig. 7 (top left), distinct and sometimes significant increases of CDNC are calculated throughout the North Atlantic- and North Pacific Oceans as well as off the southwestern coast of Africa. Close to the coasts of Northwestern Europe and California, CDNCs are increased by more than 15 %. The changes over tropical oceans are rather noisy because here, the relatively large variations in macrophysical cloud properties, such as cloud liquid water path/-geometrical thickness, dominate the signal even for the five year averages considered here.

Vertically resolved (Fig. 7, top right), we find distinct and often statistically significant changes in CDNC throughout the mid-latitude NH troposphere up to ≈ 400 hPa. Correspondingly, r_{eff} decreases, often statistically significant, throughout the mid-latitude Pacific and Atlantic Oceans as well as off the western coast of Southern Africa (Fig. 7, bottom left).

Via the parametrisation of the autoconversion (i.e. the conversion of cloud- to precipitation water after Khairoutdinov and Kogan, 2000), a response of cloud macrophysical properties to changes in CDNC is incorporated in the model. Indeed, we find the LWP to increase over large regions (Fig. 7, bottom right). Zonally averaged, the cloud cover is slightly enhanced in the NH mid-latitude boundary layer (not shown).

3.5 Impact on atmospheric radiation

For the purpose of this study, we define the AIE at TOA in terms of the "radiative flux perturbation" as given in Lohmann et al. (2010). There, the instantaneous radiation perturbation by the total aerosol loading (with cloud micro- and macrophysical properties

ACPD
12, 7073–7123, 2012

held constant), i.e. the direct total aerosol forcing, as obtained from a double-call of the ECHAM radiation scheme, is subtracted from the net all-sky radiation at TOA. By evaluating the difference of these fields with respect to the reference simulation, i.e. "experiment – *NS*", we thus obtain the changes in the net all-sky radiation as influenced only by changes in cloud micro- and macrophysical properties.

With this definition of the AIE, the results from experiment *B* yield a global, five-year mean AIE of shipping emissions at TOA of $-0.23 \pm 0.01\,\mathrm{W\,m^{-2}}$ (see Fig. 8, top left). As expected, the largest contributions come from those areas in which the change in shipping emissions leads to the largest changes in cloud micro- and macrophysical quantities.

We find the direct radiative effect (DRE) of shipping emissions at TOA, as difference between experiments *B* and *NS*, to be $-23 \pm 2\,\mathrm{mW\,m^{-2}}$ (five-year mean and interannual standard deviation). Interestingly, the DRE is distinctly positive in some parts of the semi-permanent stratocumulus fields off continental west coasts, an effect caused by absorbing aerosols from biomass burning residing above clouds (e.g., Peters et al., 2011a). The reasons for this effect in *B* are twofold. Either (1), carbonaceous aerosol from shipping emissions is lofted above the clouds or (2) the absorption of carbonaceous biomass burning aerosol from Africa above the clouds is increased due to increased internal mixing in the presence of shipping emissions. To investigate this, we compare the results from *B* to those of *BnoC* and *BnoBC* (not shown) and find that the positive DRE off the coast of Namibia and Angola can be attributed to increased internal mixing of biomass burning aerosol (see also Stier et al., 2006b).

Compared to previous estimates of the DRE from shipping emissions (−47.5 to $-9.1\,\mathrm{mW\,m^{-2}}$, Eyring et al., 2010), our value ($-23 \pm 2\,\mathrm{mW\,m^{-2}}$) is of comparable magnitude. In previous studies (e.g., Lauer et al., 2007), it is argued that the DRE of shipping emissions is negligible compared to the correspoding AIE. However, here it is evident that the emission of non-absorbing aerosols and aerosol precursors from shipping emissions have implications for the absorption characteristics of pre-existing aerosol and may lead to changes in macrophysical properties of stratocumulus fields

ACPD
12, 7073–7123, 2012

(e.g., cloud thickening as described in Wilcox, 2010).

Both the AIE and DRE represent radiative effects in the solar shortwave spectrum. It has been suggested that the aerosol influence on clouds, specifically those stemming from shipping emissions, have the potential to also alter the radiative balance at TOA in the longwave spectral range resulting from cloud deepening (e.g., Christensen and Stephens, 2011). In the results of experiment *B*, we find negligible changes in the outgoing longwave radiation (OLR) compared to experiment *NS*. However, there does seem to be a tendency towards an increase in OLR over NH mid-latitude oceans.

4 Sensitivity to uncertainties in shipping emissions

To test the models' sensitivity towards assumed emission parameters, like physical and chemical properties of emitted particles as well as the total emission amount, we performed in total seven simulations as described in Sect. 2.4. This section contains a description of the simulated responses to changes in (i) emission parametrisation, (ii) total amount of emissions and (iii) emitted amount of carbonaceous compounds from shipping emissions. The results are shown in Figs. 9, 10, 11, 12 and 13 as zonal averages. We supply a summary of globally averaged differences of selected parameters with respect to experiment *NS* in Table 4.

4.1 Effect of two different emission parametrisations

We modified the parameterisation of shipping emissions in experiment *B* in such a way that substantially more soluble particles are emitted compared to the original emission parameterisation as used in experiment *A* (see Table 2). As we show in the following, the higher number of emitted soluble particles in *B* leads to substantially different results compared to *A* with respect to aerosol processing and the subsequent effect on cloud micro- and macrophysical properties.

ACPD
12, 7073–7123, 2012

Regarding changes in species column burdens (Fig. 9), carbonaceous species are slightly more abundant in the mid-latitudes of both hemispheres in *A* compared to *B*. This may be due to regionally reduced lifetimes of carbonaceous particles in *B* – on a global scale, there is no systematic change in carbonaceous particle lifetimes (with respect to experiment *NS*) detectable (see Table 3). Due to the change in f_{SO_4}, SO_2 is less and sulfate is more abundant in *A*, respectively (see Fig. 9).

Differences in particle number column burdens (Figs. 10 and 11) are most pronounced for the modes KI and AS. For KI in *A*, particle numbers increase south of 30° S and north of 15° N due to the emission of insoluble carbonaceous particles. Between 30° S and 15° N, KI particle numbers are reduced for both experiments *A* and *B*. The most pronounced absolute decrease is simulated over South America, Sub-Sahel Africa, and Northern Australia (not shown). In these regions, carbonaceous emissions from biomass-burning are partly assigned to KI (Stier et al., 2005) and represent an efficient condensational sink regarding ship-emitted condensable species.

In experiment *A* it therefore seems that microphysical ageing of emitted KI particles over main shipping corridors is insufficient for efficient internal mixing and thus particle growth. Boundary layer nucleation is also higher in *A* compared to *B* (not shown), but boundary layer KS particle numbers are higher in *B*, indicating the inefficient microphysical ageing of emitted KI particles in *A*. The changes in AS column number burdens clearly reflect this (Fig. 11, top row). There, the relative increase obtained from *B* is distinctly higher than that of *A*, especially in the NH mid-latitudes. Less efficient internal mixing in *A* also results in longer particle lifetimes, due to reduced scavenging efficiency, and subsequent higher total column number burdens compared to *B* (not shown).

The resulting changes in zonally averaged aerosol optical depth (AOD) and its fine mode fraction (Fig. 12) match the changes in number burdens and are thus larger for *B* than for *A*. So despite the results from *A* yielding a slightly larger total aerosol number burden, *B* yields more particles in larger size modes which subsequently leads to higher AOD values. This also holds for the changes in the AOD fine mode fraction

ACPD
12, 7073–7123, 2012

because the experimental setup of *B* leads to substantially more particles in AS. The changes in the AOD of absorption are also higher for *B* due to internally mixed BC particles. The resulting aerosol direct radiative effect (DRE) is however not much different between the two experiments: $-23.5 \pm 0.9\,\mathrm{mW\,m^{-2}}$ and $-22.9 \pm 1.7\,\mathrm{mW\,m^{-2}}$ for *A* and *B*, respectively (Fig. 12, bottom right).

The relative change in zonally averaged CDNC at cloud top (Fig. 13, top left) is substantially larger in *B* than *A*, i.e. about 5 % vs. 2 % at NH mid-latitudes. Correspondingly, the r_{eff} decreases by more than 1 % in *B* versus about 0.25 % in *A* (Fig. 13, top right). The changes in cloud liquid water path (LWP) also show the same distinct difference pattern. While the LWP increases by almost 4 % over NH mid-latitudes in *B*, this increase amounts to only < 1 % in *A* (Fig. 13, bottom left).

The globally averaged AIE from *B* amounts to $-0.22 \pm 0.008\,\mathrm{W\,m^{-2}}$ whereas that of *A* is simulated at $-0.07 \pm 0.017\,\mathrm{W\,m^{-2}}$. For both simulations, the zonally averaged AIE (Fig. 13, bottom right) is largest over the NH mid-latitudes, amounting to about −0.7 and $-0.2\,\mathrm{W\,m^{-2}}$ for *B* and *A*, respectively. In experiment *B*, it is therefore the effect of assigning more and smaller soluble particles for a given amount of emissions (see Table 2) which leads to more than a tripling of the AIE in ECHAM-HAM for the model configuration we used in this study.

4.2 Effects of changes in the amount of emissions

Although we illustrated that the AIE of shipping emissions as calculated by an aerosol-climate model such as ECHAM-HAM strongly depends on the chosen emission parametrisation, we investigate a possibly more obvious AIE-determinant in this section: the uncertainty associated with total shipping emissions.

With respect to the results of experiments *A* and *B*, the results obtained from *Asc* and *Bsc* (see Sect. 2.4) show the same zonally averaged patterns for all investigated parameters, but with an offset. From experiment *Bsc*, we obtain an upper estimate of the globally averaged AIE from shipping emissions (i.e. $-0.32 \pm 0.01\,\mathrm{W\,m^{-2}}$), which is about half of the largest of previously published estimates of AIEs from shipping

ACPD
12, 7073–7123, 2012

emissions ($-0.6\,W\,m^{-2}$ as given in Lauer et al., 2007). In our experiments, the AIE does not scale linearly with the emissions, i.e. an increase of about 40 % versus a 63 % inrease in emissions compared to *B*. The non-linearity also applies to all relevant diagnostics, e.g., species burdens, particle numbers, CCN concentrations, etc. This is most probably due to saturation effects in the aerosol system (see also Stier et al., 2006a). For *Asc*, the increase in forcing scales more closely with the increase in emissions (57 % increase compared to *A*), indicating lower saturation of the aersol system compared to *B*.

4.3 Reduction of carbonaceous emissions

In the experiments *BnoBC* and *BnoC*, we set the emissions of BC and BC+POM from ships, respectively, to zero to investigate the relevance of primary carbonaceous particle emissions from ships for the calculated aerosol indirect effect. The zonally averaged relative changes of BC column burdens indicate lower values in both experiments than those of the reference experiment *NS* (Fig. 9, bottom left). This is due to increased internal mixing and the subsequently decreased lifetime of already present BC-particles. The same holds for the relative changes of POM column burden in experiment *BnoC* (Fig. 9, bottom right).

Although the number of emitted particles is surely lower in *BnoBC* and *BnoC* compared to *B*, the effect of shipping emissions on clouds and radiation is nearly the same. Analysis of mode-wise aerosol mass mixing ratios (MMRs) reveals that changes in the aerosol microphysical state are evident, especially in *BnoC*. The involved mechanisms nicely illustrate competitive effects between primary particle emission and secondary particle formation. We show zonally and meridionally averaged relative changes of selected aerosol species MMRs in experiment *BnoC* compared to *B* in Fig. 14. The depicted changes in POM-MMR for KS are also representative for the changes in BC-MMR in KS and show the expected reduction throughout the boundary layer. The model calculates an increase of sulfate particle mass NS and KS, indicating increased

ACPD
12, 7073–7123, 2012

particle nucleation in *BnoC* compared to *B*. As a result, the total aerosol number mixing ratio in AS (Fig. 14, right), i.e. the highly relevant mode for CCN formation, is about the same in both experiments. Therefore, due to the reduced number of primarily emitted carbonaceous particles, the condensational sink for sulfuric acid is reduced, leaving more ship-emitted SO_2 available for new particle formation. Interestingly, the newly formed and grown particles contribute just about as many particles to AS as the primary carbonaceous particles did, leaving the globally averaged aerosol indirect effect largely unchanged (Fig. 13, bottom left). The described effects are smaller in *BnoBC* and follow the same causality.

In recent literature, several studies have advocated the importance of accounting for carbonaceous particles in the CCN budget (e.g., Pierce et al., 2007; Spracklen et al., 2011) and that not doing so could lead to substantial underestimates of the AIE. Our results partly confirm these studies, namely that carbonaceous particles from shipping emissions play an important role in determining the CCN budget. However, we do not find that omitting carbonaceous particle emissions from ships leads to noticeably reduced AIEs due to the compensating effect of increased boundary layer nucleation. This is likely to be a consequence of their predominant emission in pristine environments (low condensational sink). Although our results represent a somewhat extreme scenario, our findings are of particular importance when considering future ship-fuel regulations, as the combustion of higher-quality ship fuel leads to less carbonaceous particle emissions compared to the currently used bunker fuels (Lack and Corbett, 2012).

Regarding changes of the DRE, the zonally averaged relative change of the AOD of absorption is reduced in *BnoBC* and *BnoC* with respect to *B*. This combines the effects of both the reduction of carbonaceous emissions from ships and the general decrease of carbonaceous-compound lifetimes. Omitting emissions of BC and POM from ships therefore results in a slightly more negative DRE compared to experiment *B* (see Table 4), highlighting the positive forcing component (at TOA) of these species.

ACPD
12, 7073–7123, 2012

5 Summary and conclusions

In this study, we used the aerosol climate model ECHAM-HAM to quantify the aerosol indirect effect (AIE) from shipping emissions. For this, we used the shipping emissions inventory from Behrens (2006) and designed the experiments to investigate the uncertainty of the derived radiative forcing (RF) associated with the uncertainty in the shipping emissions themselves. For these experiments, ECHAM-HAM was nudged with ERA-Interim re-analysis data, sea surface temperatures (SSTs) were prescribed by AMIP data, and the model integrations span the time frame of October 1999–December 2004. The first three months were used as model spin-up and discarded from the analysis.

The sensitivity experiments consisted of three sets of simulations in which the following key uncertainties/questions, with respect to AIEs, were assessed:

1. Uncertainty in the emitted particle-size distribution and -composition
2. Uncertainty in amount of emissions
3. The effect of reducing carbonaceous emissions from shipping

We addressed the first uncertainty by modifying the originally implemented emission parameterisation (AeroCom, Dentener et al., 2006). Compared to that parametrisation, we assigned all particles from shipping emissions to a soluble and/or smaller aerosol mode with a higher fraction of emitted sulfur instantaneously transformed to particulate sulfate. Thus, the modified emission parametrisation leads to the emission of substantially more soluble particles. The modifications to the emission parametrisation were within the observed ranges (see Sect. 2.4).

The second uncertainty arises from the fact that the global annual amount of fuel consumed by ship traffic is still not fully constrained. There do exist relatively low and high estimates of annual fuel consumption, with the emissions inventory we employed in this study (Behrens, 2006) providing an estimate which is on the lower end. Therefore, we scaled the emissions to meet the highest published value (see Sect. 2.4) and

ACPD
12, 7073–7123, 2012

therefore framed this emission sensitivity analysis within the range of published uncertainties.

For quantifying the third question, we performed two simulations. In the first one, only black carbon (BC) emissions from shipping were omitted and in the second one, all BC- and particulate organic matter (POM) emissions were omitted.

The different model experiments yield substantially different RFs at TOA and we found the strongest estimate of the AIE at TOA from shipping emissions to be $-0.32 \pm 0.01\,\mathrm{W\,m^{-2}}$ from the model run performed with the modified emission parametrisation and scaled emissions. This is a factor of two smaller than the upper estimate from Lauer et al. (2007), who also used the ECHAM model, but used slightly different cloud microphysics and coupled it to a different aerosol sub-model. In Lauer et al. (2007), the zonally averaged AIE is much larger in the tropics and subtropics compared to our results (Fig. 13, bottom right), yielding a substantially higher global mean value. The difference in the distribution of the forcing may have its cause in the different aerosol module and to changes in the coupling of the aerosol microphysical to the cloud microphysical parameterisations.

We found that the emission size distribution matters far more than the amount of total emissions. Even in the case of scaled emissions, the experiment with the original emission parametrisation yielded an AIE at TOA of $-0.11 \pm 0.02\,\mathrm{W\,m^{-2}}$, showing how the forcing increases by a factor of three when employing the modified emission parametrisation. This also holds for the cases with unscaled emissions, where the experiments employing the original- and modified parametrisation yield an AIE at TOA of $-0.07 \pm 0.017\,\mathrm{W\,m^{-2}}$ and $-0.23 \pm 0.008\,\mathrm{W\,m^{-2}}$, respectively.

We recognised that carbonaceous particle emissions from ships play an important role in determining the boundary layer CCN budget. However, omitting carbonaceous aerosol from the shipping emissions proved not to have a substantial impact on the obtained AIE as suggested by studies advocating the importance of accounting for carbonaceous CCN (e.g., Pierce et al., 2007; Spracklen et al., 2011). This is because in our model, omitting carbonaceous particle emissions from ships lead to enhanced

ACPD
12, 7073–7123, 2012

boundary-layer new particle formation, which is likely to be a consequence of their predominant emission in pristine environments (low condensational sink), favourable for aerosol nucleation. This compensated for the reduced primary particle emissions, leaving the globally averaged AIE nearly unaltered.

Acknowledgements. The authors thank Ulrike Niemeier (MPI-M) for reviewing an earlier version of this manuscript. Kai Zhang and Sebastian Rast (MPI-M) assisted with performing the simulations. The shipping emission inventory was provided in the framework of of the European Union FP6 Integrated Project QUANTIFY. The model simulations were performed at the German High Performance Computing Centre for Climate and Earth System Research (Deutsches Klimarechenzentrum, DKRZ). K. Peters was partly funded by the European Union FP6 Integrated Project QUANTIFY and by the European Commission under the EU Seventh Research Framework Programme (grant 218793, MACC) and acknowledges the funding support from the Guest-Exchange program of the International Max Planck Research School on Earth System Modelling (IMPRS-ESM) for supporting his visit to the University of Oxford. UK. P. Stier was partly supported by the UK NERC AEROS project (NE/G006148/1). The work of J. Quaas was funded by the German Research Foundation (DFG) in an "Emmy Noether" grant.

The service charges for this open access publication have been covered by the Max Planck Society.

References

Agrawal, H., Malloy, Q., Welch, W., Wayne Miller, J., and Cocker III, D.: In-use gaseous and particulate matter emissions from a modern ocean going container vessel, Atmos. Environ., 42, 5504–5510, doi:10.1016/j.atmosenv.2008.02.053, 2008. 7083

Albrecht, B. A.: Aerosols, cloud microphysics, and fractional cloudiness, Science, 245, 1227–1230, 1989. 7075

Ångström, A.: Atmospheric turbidity, global illumination and planetary albedo of the earth, Tellus, 14, 435–450, 1962. 7075

Balkanski, Y., Myhre, G., Gauss, M., Rädel, G., Highwood, E. J., and Shine, K. P.: Direct

ACPD

12, 7073–7123, 2012

radiative effect of aerosols emitted by transport: from road, shipping and aviation, Atmos. Chem. Phys., 10, 4477–4489, doi:10.5194/acp-10-4477-2010, 2010. 7077
Behrens, H. L.: Present Traffic and Emissions from Maritime Shipping, in: Deliverable D1.1.2.2 of the EU-IP QUANTIFY (confidential), Det Norske Veritas, available at: http://www.pa.op.dlr.de/quantify/, 2006. 7081, 7096, 7106, 7110, 7111
Bond, T.: Can warming particles enter global climate discussions?, Environ. Res. Lett., 2, 045030, doi:10.1088/1748-9326/2/4/045030, 2007. 7076
Bond, T., Streets, D., Yarber, K., Nelson, S., Woo, J., and Klimont, Z.: A technology-based global inventory of black and organic carbon emissions from combustion, J. Geophys. Res., 109, D14203, doi:10.1029/2003JD003697, 2004. 7080
Borken-Kleefeld, J., Berntsen, T., and Fuglestvedt, J.: Specific climate impact of passenger and freight transport, Environ. Sci. Technol., 44, 5700–5706, doi:10.1021/es9039693, 2010. 7076
Buhaug, Ø., Corbett, J. J., Endresen, Ø., Eyring, V., Faber, J., Hanayama, S., Lee, D. S., Lee, D., Lindstad, H., Markowska, A. Z., Mjelde, A., Nelissen, D., Nilsen, J., Pålsson, C., Winebrake, J. J., Wu, W.Q., and Yoshida, K.: Second IMO GHG study 2009, International Maritime Organization (IMO), London, UK, 24, 2009. 7076
Capaldo, K., Corbett, J., Kasibhatla, P., Fischbeck, P., and Pandis, S.: Effects of ship emissions on sulphur cycling and radiative climate forcing over the ocean, Nature, 400, 743–746, 1999. 7077
Christensen, M. and Stephens, G.: Microphysical and macrophysical responses of marine stratocumulus polluted by underlying ships: evidence of cloud deepening, J. Geophys. Res.-Atmos., 116, D03201, doi:10.1029/2010JD014638, 2011. 7091
Corbett, J. and Koehler, H.: Updated emissions from ocean shipping, J. Geophys. Res., 108, 4650–4664, 2003. 7081, 7084
Corbett, J. and Koehler, H.: Considering alternative input parameters in an activity-based ship fuel consumption and emissions model: reply to comment by Øyvind Endresen et al. on Updated emissions from ocean shipping, J. Geophys. Res., 109, D23303, doi:10.1029/2004JD005030, 2004. 7081
Corbett, J., Fischbeck, P., and Pandis, S.: Global nitrogen and sulfur inventories for oceangoing ships, J. Geophys. Res., 104, 3457–3470, doi:10.1029/1998JD100040, 1999. 7077
Dalsøren, S. B., Eide, M. S., Endresen, Ø., Mjelde, A., Gravir, G., and Isaksen, I. S. A.: Update on emissions and environmental impacts from the international fleet of ships: the contribution

ACPD
12, 7073–7123, 2012

from major ship types and ports, Atmos. Chem. Phys., 9, 2171–2194, doi:10.5194/acp-9-2171-2009, 2009. 7081

Dentener, F., Kinne, S., Bond, T., Boucher, O., Cofala, J., Generoso, S., Ginoux, P., Gong, S., Hoelzemann, J. J., Ito, A., Marelli, L., Penner, J. E., Putaud, J.-P., Textor, C., Schulz, M., van der Werf, G. R., and Wilson, J.: Emissions of primary aerosol and precursor gases in the years 2000 and 1750 prescribed data-sets for AeroCom, Atmos. Chem. Phys., 6, 4321–4344, doi:10.5194/acp-6-4321-2006, 2006. 7080, 7096, 7106, 7110, 7111

Devasthale, A., Krüger, O., and Grassl, H.: Change in cloud-top temperatures over Europe, IEEE Geosci. Remote S., 2, 333–336, doi:10.1109/LGRS.2005.851736, 2005. 7075

Devasthale, A., Krüger, O., and Grassl, H.: Impact of ship emissions on cloud properties over coastal areas, Geophys. Res. Lett., 33, L02811, doi:10.1029/2005GL024470, 2006. 7077

Endresen, Ø., Sørgård, E., Sundet, J., Dalsøren, S., Isaksen, I., Berglen, T., and Gravir, G.: Emission from international sea transportation and environmental impact, J. Geophys. Res., 108, 4560, doi:10.1029/2002JD002898, 2003. 7081

Endresen, Ø., Sørgård, E., Bakke, J., and Isaksen, I.: Substantiation of a lower estimate for the bunker inventory: comment on updated emissions from ocean shipping by James J. Corbett and Horst W. Koehler, J. Geophys. Res., 109, D23302, doi:10.1029/2004JD004853, 2004. 7081, 7083

Eyring, V., Köhler, H., Lauer, A., and Lemper, B.: Emissions from international shipping: 2. Impact of future technologies on scenarios until 2050, J. Geophys. Res., 110, D17306, doi:10.1029/2004JD005620, 2005a. 7076

Eyring, V., Köhler, H., Van Aardenne, J., and Lauer, A.: Emissions from international shipping: 1. The last 50 years, J. Geophys. Res., 110, D17305, doi:10.1029/2004JD005619, 2005b. 7076, 7081

Eyring, V., Stevenson, D. S., Lauer, A., Dentener, F. J., Butler, T., Collins, W. J., Ellingsen, K., Gauss, M., Hauglustaine, D. A., Isaksen, I. S. A., Lawrence, M. G., Richter, A., Rodriguez, J. M., Sanderson, M., Strahan, S. E., Sudo, K., Szopa, S., van Noije, T. P. C., and Wild, O.: Multi-model simulations of the impact of international shipping on Atmospheric Chemistry and Climate in 2000 and 2030, Atmos. Chem. Phys., 7, 757–780, doi:10.5194/acp-7-757-2007, 2007. 7077

Eyring, V., Isaksen, I. S. A., Berntsen, T., Collins, W. J., Corbett, J. J., Endresen, O., Grainger, R. G., Moldanova, J., Schlager, H., and Stevenson, D. S.: Transport impacts on atmosphere and climate: shipping, Atmos. Environ., 44, 4735–4771,

ACPD
12, 7073–7123, 2012

doi:10.1016/j.atmosenv.2009.04.059, 2010. 7078, 7090
Feichter, J., Kjellström, E., Rodhe, H., Dentener, F., Lelieveldi, J., and Roelofs, G.: Simulation of the tropospheric sulfur cycle in a global climate model, Atmos. Environ., 30, 1693–1707, 1996. 7079
Forster, P., Ramaswamy, V., Artaxo, P., Berntsen, T., Betts, R., Fahey, D. W., Haywood, J., Lean, J., Lowe, D. C., Myhre, G., Nganga, J., Prinn, R., Raga, G., Schulz, M., and Van Dorland, R.: Changes in atmospheric constituents and in radiative forcing, in: Climate Change 2007: The Physical Science Basis. Contribution of Working Group I to the Fourth Assessment Report of the Intergovernmental Panel on Climate Change, edited by: Solomon, S., Qin, D., Manning, M., Chen, Z., Marquis, M., Averyt, K. B., Tignor, M., and Miller, H. L., Cambridge University Press, Cambridge, United Kingdom and New York, NY, USA, 2007. 7075
Fuglestvedt, J., Berntsen, T., Eyring, V., Isaksen, I., Lee, D. S., and Sausen, R.: Shipping emissions: from cooling to warming of climate – and reducing impacts on health, Environ. Sci. Technol., 43, 9057–9062, doi:10.1021/es901944r, 2009. 7078
Guelle, W., Schulz, M., Balkanski, Y., and Dentener, F.: Influence of the source formulation on modeling the atmospheric global distribution of sea salt aerosol, J. Geophys. Res., 106, 27509–27524, 2001. 7080
Horowitz, L., Walters, S., Mauzerall, D., Emmons, L., Rasch, P., Granier, C., Tie, X., Lamarque, J., Schultz, M., Tyndall, G., Orlando, J. J., and Brasseur, G. P.: A global simulation of tropospheric ozone and related tracers: description and evaluation of MOZART, version 2, J. Geophys. Res., 108, 4784, doi:10.1029/2002JD002853, 2003. 7080, 7086
IMO: Regulations for the prevention of air pollution from ships and NO_x technical code, ANNEX IV of MARPOL 73/78, Tech. rep., London, 1998. 7077
Kazil, J. and Lovejoy, E. R.: A semi-analytical method for calculating rates of new sulfate aerosol formation from the gas phase, Atmos. Chem. Phys., 7, 3447–3459, doi:10.5194/acp-7-3447-2007, 2007. 7079
Kazil, J., Stier, P., Zhang, K., Quaas, J., Kinne, S., O'Donnell, D., Rast, S., Esch, M., Ferrachat, S., Lohmann, U., and Feichter, J.: Aerosol nucleation and its role for clouds and Earth's radiative forcing in the aerosol-climate model ECHAM5-HAM, Atmos. Chem. Phys., 10, 10733–10752, doi:10.5194/acp-10-10733-2010, 2010. 7079, 7086
Kettle, A. and Andreae, M.: Flux of dimethylsulfide from the oceans – a comparison of updated data sets and flux models, J. Geophys. Res., 105, 793–808, 2000. 7080

ACPD
12, 7073–7123, 2012

Khairoutdinov, M. and Kogan, Y.: A new cloud physics parameterization in a large-eddy simulation model of marine stratocumulus, Mon. Weather Rev., 128, 229–243, 2000. 7080, 7089

Kinne, S., Schulz, M., Textor, C., Guibert, S., Balkanski, Y., Bauer, S. E., Berntsen, T., Berglen, T. F., Boucher, O., Chin, M., Collins, W., Dentener, F., Diehl, T., Easter, R., Feichter, J., Fillmore, D., Ghan, S., Ginoux, P., Gong, S., Grini, A., Hendricks, J., Herzog, M., Horowitz, L., Isaksen, I., Iversen, T., Kirkevåg, A., Kloster, S., Koch, D., Kristjansson, J. E., Krol, M., Lauer, A., Lamarque, J. F., Lesins, G., Liu, X., Lohmann, U., Montanaro, V., Myhre, G., Penner, J., Pitari, G., Reddy, S., Seland, O., Stier, P., Takemura, T., and Tie, X.: An AeroCom initial assessment – optical properties in aerosol component modules of global models, Atmos. Chem. Phys., 6, 1815–1834, doi:10.5194/acp-6-1815-2006, 2006. 7080

Kireeva, E., Popovicheva, O., Persiantseva, N., Timofeyev, M., and Shonija, N.: Fractionation analysis of transport engine-generated soot particles with respect to hygroscopicity, J. Atmos. Chem., 64, 129–147, doi:10.1007/s10874-010-9173-y, 2010. 7083

Koch, D. and Del Genio, A. D.: Black carbon semi-direct effects on cloud cover: review and synthesis, Atmos. Chem. Phys., 10, 7685–7696, doi:10.5194/acp-10-7685-2010, 2010. 7076

Koren, I., Kaufman, Y., Rosenfeld, D., Remer, L., and Rudich, Y.: Aerosol invigoration and restructuring of Atlantic convective clouds, Geophys. Res. Lett., 32, L14828, doi:10.1029/2005GL023187, 2005. 7075

Kulmala, M., Lehtinen, K. E. J., and Laaksonen, A.: Cluster activation theory as an explanation of the linear dependence between formation rate of 3nm particles and sulphuric acid concentration, Atmos. Chem. Phys., 6, 787–793, doi:10.5194/acp-6-787-2006, 2006. 7079

Kyoto Protocol: Kyoto Protocol to the United Nations Framework Convention on Climate Change, United Nations Publications, Geneva, Switzerland, 1997. 7076

Lack, D. A. and Corbett, J. J.: Black carbon from ships: a review of the effects of ship speed, fuel quality and exhaust gas scrubbing, Atmos. Chem. Phys. Discuss., 12, 3509–3554, doi:10.5194/acpd-12-3509-2012, 2012. 7078, 7084, 7095

Lack, D. A., Corbett, J. J., Onasch, T., Lerner, B., Massoli, P., Quinn, P. K., Bates, T. S., Covert, D. S., Coffman, D., Sierau, B., Herndon, S., Allan, J., Baynard, T., Lovejoy, E., Ravishankara, A. R., and Williams, E.: Particulate emissions from commercial shipping: chemical, physical, and optical properties, J. Geophys. Res.-Atmos., 114, D00F04, doi:10.1029/2008JD011300, 2009. 7083

Lauer, A., Eyring, V., Hendricks, J., Jöckel, P., and Lohmann, U.: Global model simulations

ACPD
12, 7073–7123, 2012

of the impact of ocean-going ships on aerosols, clouds, and the radiation budget, Atmos. Chem. Phys., 7, 5061–5079, doi:10.5194/acp-7-5061-2007, 2007. 7077, 7084, 7090, 7094, 7097

Lauer, A., Eyring, V., Corbett, J., Wang, C., and Winebrake, J.: Assessment of near-future policy instruments for oceangoing shipping: impact on atmospheric aerosol burdens and the Earth's radiation budget, Environ. Sci. Technol., 43, 5592–5598, doi:10.1021/es900922h, 2009. 7077, 7078

Lin, S. and Rood, R.: Multidimensional flux-form semi-Lagrangian transport schemes, Mon. Weather Rev., 124, 2046–2070, 1996. 7079

Lohmann, U., Stier, P., Hoose, C., Ferrachat, S., Kloster, S., Roeckner, E., and Zhang, J.: Cloud microphysics and aerosol indirect effects in the global climate model ECHAM5-HAM, Atmos. Chem. Phys., 7, 3425–3446, doi:10.5194/acp-7-3425-2007, 2007. 7079, 7080

Lohmann, U., Rotstayn, L., Storelvmo, T., Jones, A., Menon, S., Quaas, J., Ekman, A. M. L., Koch, D., and Ruedy, R.: Total aerosol effect: radiative forcing or radiative flux perturbation?, Atmos. Chem. Phys., 10, 3235–3246, doi:10.5194/acp-10-3235-2010, 2010. 7089

Myhre, G.: Consistency between satellite-derived and modeled estimates of the direct aerosol effect, Science, 325, 187, doi:10.1126/science.1174461, 2009. 7075

Olivier, J. G. J., Van Aardenne, J. A., Dentener, F. J., Pagliari, V., Ganzeveld, L. N., and Peters, J. A. H. W.: Recent trends in global greenhouse gas emissions:regional trends 1970–2000 and spatial distributionof key sources in 2000, Environm. Sci., 2, 81–99, doi:10.1080/15693430500400345, 2005. 7080, 7106, 7110

Peters, K., Quaas, J., and Bellouin, N.: Effects of absorbing aerosols in cloudy skies: a satellite study over the Atlantic Ocean, Atmos. Chem. Phys., 11, 1393–1404, doi:10.5194/acp-11-1393-2011, 2011. 7075, 7090

Peters, K., Quaas, J., and Graßl, H.: A search for large-scale effects of ship emissions on clouds and radiation in satellite data, J. Geophys. Res.-Atmos., 116, D24205, doi:10.1029/2011JD016531, 2011b. 7076, 7077

Petzold, A., Hasselbach, J., Lauer, P., Baumann, R., Franke, K., Gurk, C., Schlager, H., and Weingartner, E.: Experimental studies on particle emissions from cruising ship, their characteristic properties, transformation and atmospheric lifetime in the marine boundary layer, Atmos. Chem. Phys., 8, 2387–2403, doi:10.5194/acp-8-2387-2008, 2008. 7076, 7083

Pierce, J. R. and Adams, P. J.: Uncertainty in global CCN concentrations from uncertain aerosol nucleation and primary emission rates, Atmos. Chem. Phys., 9, 1339–1356,

ACPD
12, 7073–7123, 2012

doi:10.5194/acp-9-1339-2009, 2009. 7087
Pierce, J. R., Chen, K., and Adams, P. J.: Contribution of primary carbonaceous aerosol to cloud condensation nuclei: processes and uncertainties evaluated with a global aerosol microphysics model, Atmos. Chem. Phys., 7, 5447–5466, doi:10.5194/acp-7-5447-2007, 2007. 7076, 7095, 7097
Quaas, J., Ming, Y., Menon, S., Takemura, T., Wang, M., Penner, J. E., Gettelman, A., Lohmann, U., Bellouin, N., Boucher, O., Sayer, A. M., Thomas, G. E., McComiskey, A., Feingold, G., Hoose, C., Kristjánsson, J. E., Liu, X., Balkanski, Y., Donner, L. J., Ginoux, P. A., Stier, P., Grandey, B., Feichter, J., Sednev, I., Bauer, S. E., Koch, D., Grainger, R. G., Kirkevåg, A., Iversen, T., Seland, Ø., Easter, R., Ghan, S. J., Rasch, P. J., Morrison, H., Lamarque, J.-F., Iacono, M. J., Kinne, S., and Schulz, M.: Aerosol indirect effects – general circulation model intercomparison and evaluation with satellite data, Atmos. Chem. Phys., 9, 8697–8717, doi:10.5194/acp-9-8697-2009, 2009. 7075
Schreier, M., Mannstein, H., Eyring, V., and Bovensmann, H.: Global ship track distribution and radiative forcing from 1 year of AATSR data, Geophys. Res. Lett., 34, L17814, doi:10.1029/2007GL030664, 2007. 7076
Simmons, A., Uppala, S., Dee, D., and Kobayashi, S.: ERA-interim: new ECMWF reanalysis products from 1989 onwards, ECMWF Newsletter, 110, 25–35, 2007. 7079
Small, J., Chuang, P., Feingold, G., and Jiang, H.: Can aerosol decrease cloud lifetime?, Geophys. Res. Lett., 36, L16806, doi:10.1029/2009GL038888, 2009. 7075
Spracklen, D. V., Carslaw, K. S., Pöschl, U., Rap, A., and Forster, P. M.: Global cloud condensation nuclei influenced by carbonaceous combustion aerosol, Atmos. Chem. Phys., 11, 9067–9087, doi:10.5194/acp-11-9067-2011, 2011. 7076, 7095, 7097
Stevens, B. and Feingold, G.: Untangling aerosol effects on clouds and precipitation in a buffered system, Nature, 461, 607–613, doi:10.1038/nature08281, 2009. 7075
Stier, P., Feichter, J., Kinne, S., Kloster, S., Vignati, E., Wilson, J., Ganzeveld, L., Tegen, I., Werner, M., Balkanski, Y., Schulz, M., Boucher, O., Minikin, A., and Petzold, A.: The aerosol-climate model ECHAM5-HAM, Atmos. Chem. Phys., 5, 1125–1156, doi:10.5194/acp-5-1125-2005, 2005. 7092
Stier, P., Feichter, J., Kloster, S., Vignati, E., and Wilson, J.: Emission-induced nonlinearities in the global aerosol system: results from the ECHAM5-HAM aerosol-climate model, J. Climate, 19, 3845–3862, 2006a. 7094
Stier, P., Seinfeld, J. H., Kinne, S., Feichter, J., and Boucher, O.: Impact of nonabsorbing an-

ACPD
12, 7073–7123, 2012

thropogenic aerosols on clear-sky atmospheric absorption, J. Geophys. Res., 111, D18201, doi:10.1029/2006JD007147, 2006b. 7090
Stier, P., Grandey, B., West, R., Lohmann, U., Quaas, J., and Seinfeld, J.: Observational constraints on mechanistic aerosol-cloud coupling in the microphysical aeroso-climate model ECHAM5-HAM, Atmos. Chem. Phys. Discuss., in preparation, 2012. 7080
Sundqvist, H., Berge, E., and Kristjansson, J.: Condensation and cloud parameterization studies with a mesoscale numerical weather prediction model, Mon. Weather Rev., 117, 1641–1657, 1989. 7078, 7080
Taylor, K., Williamson, D., and Zwiers, F.: The sea surface temperature and sea-ice concentration boundary conditions for AMIP II simulations, PCMDI Rep., 60, 28, 2000. 7082
Tegen, I., Harrison, S., Kohfeld, K., Prentice, I., Coe, M., and Heimann, M.: Impact of vegetation and preferential source areas on global dust aerosol: results from a model study, J. Geophys. Res., 107, 4576, doi:10.1029/2001JD000963, 2002. 7080
Tiedtke, M.: A comprehensive mass flux scheme for cumulus parameterization in large-scale models, Mon. Weather Rev., 117, 1779–1800, 1989. 7079
Twomey, S.: Pollution and the planetary albedo, Atmos. Environ., 8, 1251–1256, 1974. 7075
Vignati, E., Wilson, J., and Stier, P.: M7: An efficient size-resolved aerosol microphysics module for large-scale aerosol transport models, J. Geophys. Res., 109, D22202, doi:10.1029/2003JD004485, 2004. 7079
Wang, C., Corbett, J., and Firestone, J.: Improving spatial representation of global ship emissions inventories, Environ. Sci. Technol., 42, 193–199, doi:10.1021/es0700799, 2007. 7081
Wilcox, E. M.: Stratocumulus cloud thickening beneath layers of absorbing smoke aerosol, Atmos. Chem. Phys., 10, 11769–11777, doi:10.5194/acp-10-11769-2010, 2010. 7091
Zhang, K., O'Donnell, D., Kazil, J., Stier, P., Kinne, S., Lohmann, U., Ferrachat, S., Croft, B., Quaas, J., Wan, H., Rast, S., and Feichter, J.: The global aerosol-climate model ECHAM-HAM, version 2: sensitivity to improvements in process prepresentations, submitted, 2012. 7078, 7079

ACPD
12, 7073–7123, 2012

Table 1. Total annual mean emissions from seagoing ships of particulate matter and aerosol precursors in ($Tg\,yr^{-1}$) for the year 2000. The QUANTIFY inventory is the one employed in this study; values for the AeroCom inventory (Olivier et al., 2005; Dentener et al., 2006) are shown for reference purposes.

Compound	QUANTIFY (Behrens, 2006)	AeroCom (Olivier et al., 2005; Dentener et al., 2006)
SO_2	7.95	7.75
BC	0.03	0.13
POM	0.15	0.06

ACPD
12, 7073–7123, 2012

Table 2. Experimental setup configurations for the performed GCM runs. The "old" emission parameterisation refers to the operational AeroCom method whereas the "new" one was developed in this study. The scaling factor is applied to investigate the range of uncertainty associated with unknown total fuel consumption. The acronyms for the emission modes are: KI (Aitken insoluble), KS (Aitken soluble), AS (Accumulation soluble), CS (Coarse soluble). f_{SO_4} denotes the mass fraction of emitted sulfur to be emitted as primary sulfate. HAM treats OC emissions as emissions of POM. OC emissions are therefore scaled by 1.4 to obtain values of emitted POM. The approximate number of emitted soluble particles s^{-1} is shown to illustrate the effect of the applied model changes.

Experiment	emission paremeterisation	scale factor	Particulate emissions, emission mode f_{SO_4}	BC	OC (POM)	≈ # of emitted sol. particles (s^{-1})
NS	old	–	–	–	–	–
A	old	1	2.5 % (50 % AS, 50 % CS)	KI	KI	4.8×10^{17}
B	new	1	4.5 %, KS	KS	KS	8×10^{19}
Asc	old	1.63	2.5 % (50 % AS, 50 % CS)	KI	KI	7.8×10^{17}
Bsc	new	1.63	4.5 %, KS	KS	KS	1.3×10^{20}
BnoBC	new	1	4.5 %, KS	–	KS	7.6×10^{19}
BnoC	new	1	4.5 %, KS	–	–	5.5×10^{19}

ACPD
12, 7073–7123, 2012

Table 3. Atmospheric lifetimes of the aerosol species considered in ECHAM-HAM in experiment *NS* [d] and changes in the remaining experiments with respect to *NS* (min). The lifetime is defined as the ratio of total burden over total sources. All aerosol species treated in ECHAM-HAM are considered here, i.e. sulfate, black carbon (BC), particulate organic matter (POM), sea salt (SS) and dust (DU).

Compound	*NS*	*A*	*B*	*Asc*	*Bsc*	*BnoBC*	*BnoC*
sulfate	4.8 ± 0.16	−7.9 ± 2.7	−30.5 ± 3.5	−32.8 ± 6.3	−18.9 ± 4.3	−29.2 ± 5.5	0.3 ± 1.9
BC	6.3 ± 0.17	−3.9 ± 7.2	−17.8 ± 12.1	−16 ± 10.2	−16.7 ± 8.5	−4 ± 3.3	10.2 ± 13.2
POM	6.1 ± 0.19	−7.6 ± 9.6	−2.7 ± 17	−11.5 ± 14.7	−8.4 ± 13.2	−10.4 ± 2.6	−4.9 ± 19.2
SS	0.7 ± 0.006	−1.6 ± 0.1	2.3 ± 0.1	−1.3 ± 0.1	0.9 ± 0.1	2.2 ± 0.3	−0.06 ± 0.1
DU	4.9 ± 0.2	1.6 ± 7.2	−19 ± 6.2	−11.5 ± 11.8	−14.3 ± 11.5	−19 ± 9	2.3 ± 8.9

ACPD
12, 7073–7123, 2012

Table 4. Globally averaged changes of aerosol- and cloud properties for the experiments described in Sect. 2.4 with respect to experiment *NS*, i.e. "experiment – *NS*". The results for cloud droplet number concentration (CDNC) and cloud droplet effective radius (r_{eff}) represent values at cloud top as diagnosed by the model. The values in parantheses represent globally averaged relative changes in % as $\left(\frac{B-NS}{NS}\cdot 100\right)$.

	AOD	AOD FMF	ADE ($\mathrm{mW\,m^{-2}}$)	CDNC ($\mathrm{cm^{-3}}$)	r_{eff} (µm)	LWP ($\mathrm{kg\,m^{-2}}$)	AIE ($\mathrm{W\,m^{-2}}$)
A	1.9E-3 ± 0.07E-3 (1.51 ± 0.02)	4.6E-3 ± 0.1E-3 (0.86 ± 0.03)	−23.5 ± 0.9	0.84 ± 0.05 (3.12 ± 0.2)	−0.03 ± 0.003 (−0.07 ± 0.04)	6.6E-4 ± 0.6E-4 (0.61 ± 0.05)	−0.07 ± 0.017
B	2.3E-3 ± 0.1E-3 (1.87 ± 0.04)	5.4E-3 ± 0.08E-3 (1 ± 0.02)	−23 ± 1.7	1.64 ± 0.18 (4.5 ± 0.3)	−0.07 ± 0.006 (−0.37 ± 0.05)	2E-3 ± 0.06E-3 (1.43 ± 0.05)	−0.23 ± 0.008
Asc	3E-3 ± 0.07E-3 (2.47 ± 0.04)	7.3E-3 ± 0.02E-3 (1.36 ± 0.04)	−38 ± 1.5	1.24 ± 0.17 (3.65 ± 0.29)	−0.04 ± 0.009 (−0.15 ± 0.08)	1E-3 ± 0.05E-3 (0.94 ± 0.05)	−0.11 ± 0.02
Bsc	3.7E-3 ± 0.13E-3 (3 ± 0.06)	8.7E-3 ± 0.15E-3 (1.62 ± 0.05)	−37.4 ± 1.6	2.6 ± 0.2 (6.13 ± 0.34)	−0.09 ± 0.005 (−0.58 ± 0.04)	3E-3 ± 0.1E-3 (2 ± 0.07)	−0.32 ± 0.01
BnoBC	2.3E-3 ± 0.07E-3 (1.86 ± 0.02)	5.3E-3 ± 0.1E-3 (1 ± 0.02)	−24.1 ± 0.7	1.57 ± 0.08 (4.34 ± 0.21)	−0.06 ± 0.004 (−0.33 ± 0.03)	2E-3 ± 0.1E-3 (1.37 ± 0.12)	−0.21 ± 0.02
BnoC	2.3E-3 ± 0.1E-3 (1.83 ± 0.05)	5.1E-3 ± 0.1E-3 (0.95 ± 0.03)	−23.9 ± 1.4	1.8 ± 0.14 (4.88 ± 0.3)	−0.06 ± 0.007 (−0.35 ± 0.06)	2.1E-3 ± 0.09E-3 (1.41 ± 0.08)	−0.22 ± 0.02

ACPD
12, 7073–7123, 2012

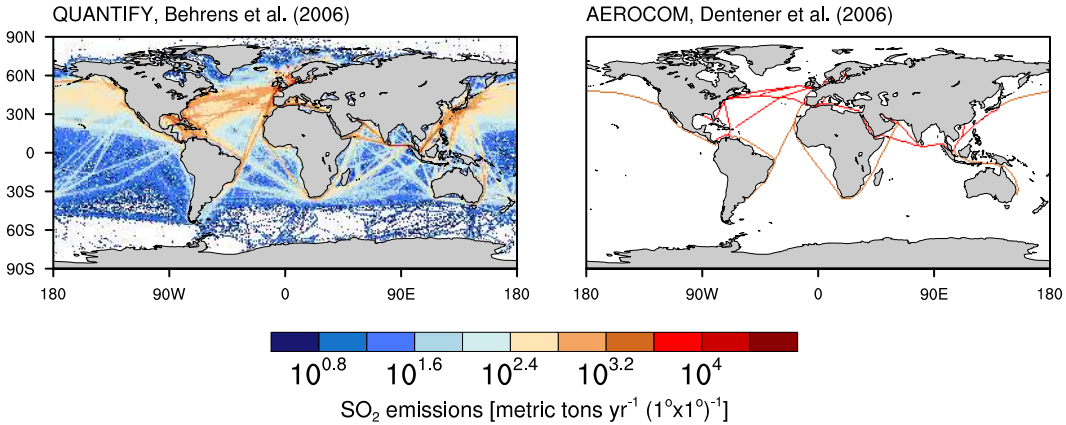

Fig. 1. Emission fluxes of SO_2 from ships as in the QUANTIFY- and AeroCom emission inventories for the year 2000 (Olivier et al., 2005; Behrens, 2006; Dentener et al., 2006).

ACPD
12, 7073–7123, 2012

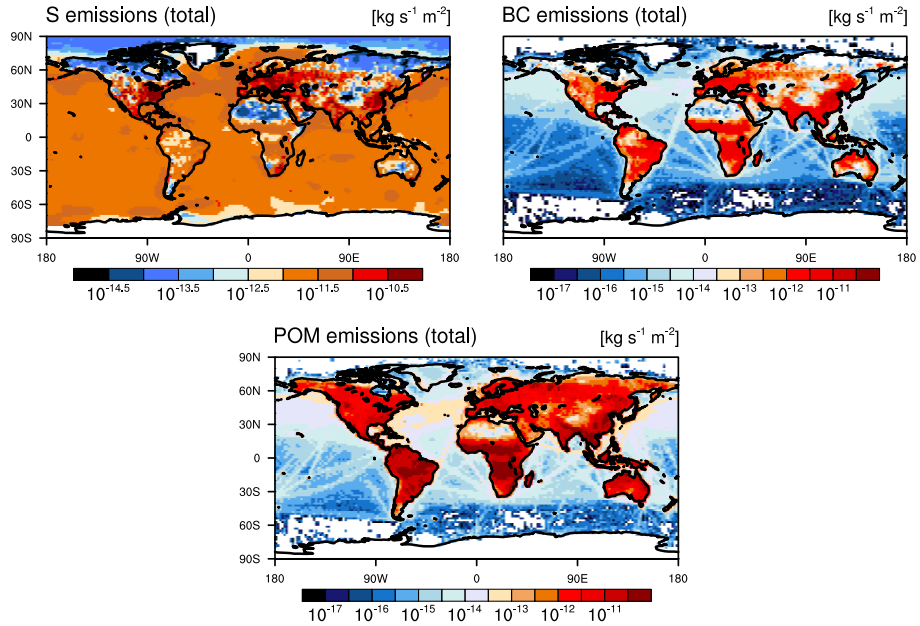

Fig. 2. Total emissions of aerosols and aerosol precursors as used in experiment setup *B*. Top left: sulphur (comprised of sulphur dioxide (SO_2), sulfate and DMS); Top right: BC; Bottom: particulate organic matter (POM). The colour scales denote the $\log_{10}$ of emission fluxes in ($kg\,s^{-1}\,m^{-2}$). Emissions over land correspond to those prescribed in AeroCom (Dentener et al., 2006), anthropogenic emissions over water surfaces to those provided in the QUANTIFY shipping emission inventory (Behrens, 2006).

ACPD
12, 7073–7123, 2012

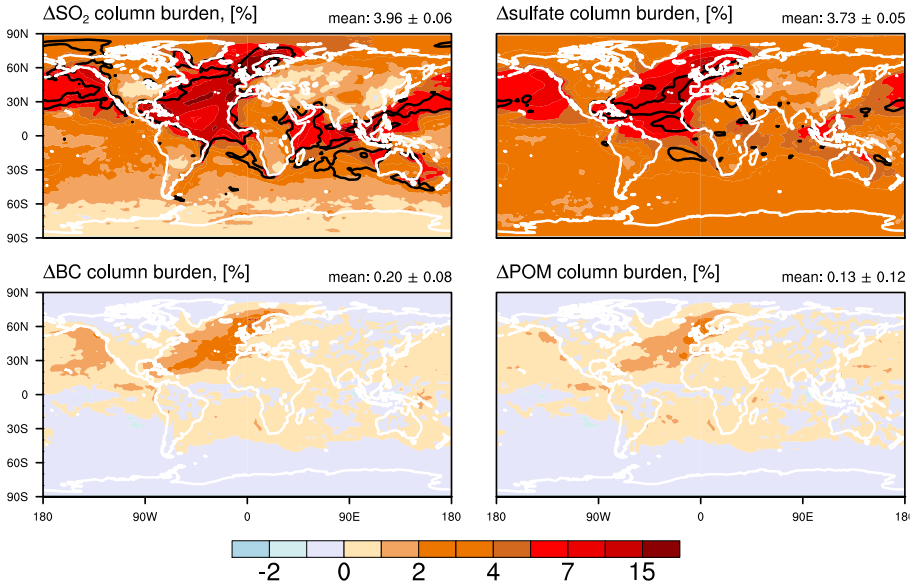

Fig. 3. Relative changes in (%) of column burden of sulphur dioxide (SO_2, top left), sulfate (top right), black carbon (BC, bottom left) and particulate organic matter (POM, bottom right) in experiment B compared to experiment *NS* (derived from $\frac{B-NS}{NS} \cdot 100$). The black contour lines enclose areas showing statistical significance at the 90 % level.

ACPD
12, 7073–7123, 2012

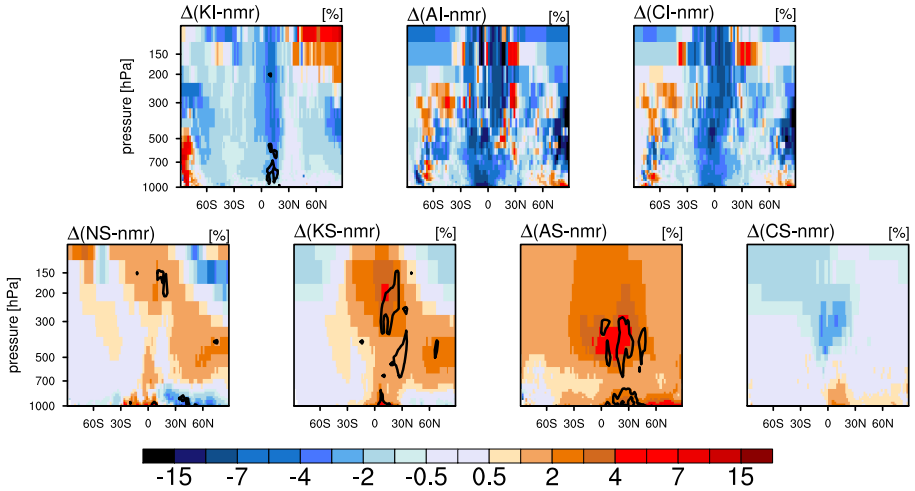

Fig. 4. Zonal annual mean relative changes in (%) of particle number mixing ratios (nmr) in experiment *B* compared to experiment *NS* (derived from $\frac{B-NS}{NS} \cdot 100$). The change of particle number concentration in each aerosol mode, as resolved by ECHAM-HAM, is shown. The acronyms in the plot captions denote the respective aerosol mode in HAM and are as follows: KI (aitKen Insoluble), AI (Accumulation Insoluble), CI (Coarse Insoluble), NS (Nucleation Soluble), KS (aitKen Soluble), AS (Accumulation Soluble), CS (Coarse Soluble). The black contour lines enclose areas showing statistical significance at the 90 % level.

ACPD
12, 7073–7123, 2012

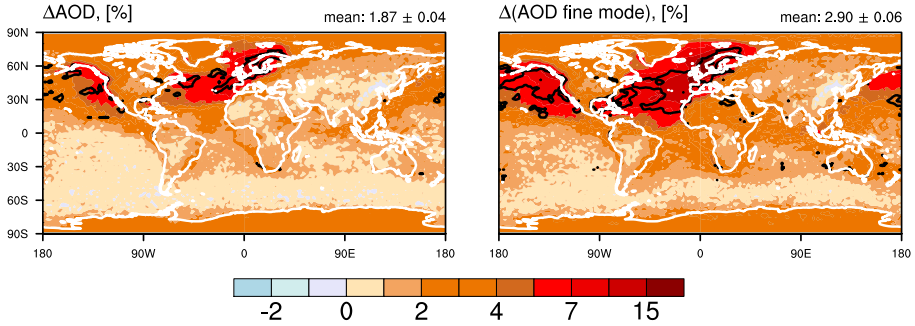

Fig. 5. Relative changes in (%) of aerosol optical depth (AOD, left) and its fine mode (right) in experiment *B* compared to experiment *NS* $\left(\text{derived from } \frac{B-NS}{NS} \cdot 100\right)$. The black contour lines enclose areas showing statistical significance at the 90 % level.

ACPD
12, 7073–7123, 2012

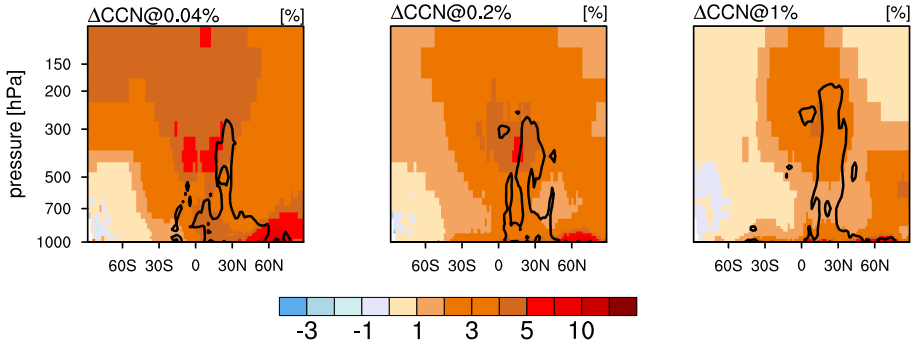

Fig. 6. Relative changes in (%) of the temporally- and zonaly averaged cloud condensation nuclei (CCN) concentrations at supersaturations $S = 0.04\,\%$ (left), $S = 0.2\,\%$ (middle) and $S = 1\,\%$ (right) in experiment *B* compared to experiment *NS* (derived from $\frac{B-NS}{NS} \cdot 100$). The black contour lines enclose areas showing statistical significance at the 90 % level.

ACPD
12, 7073–7123, 2012

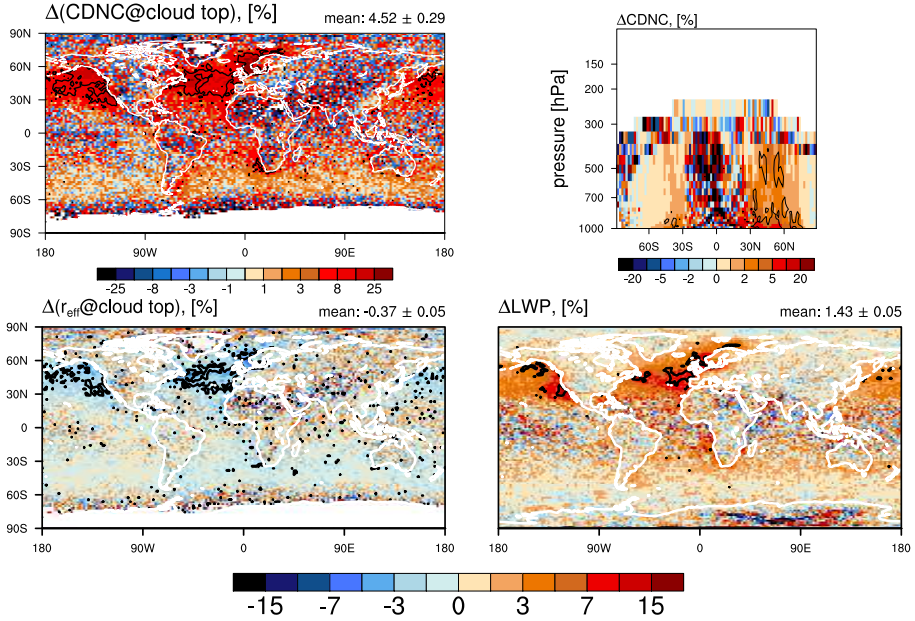

Fig. 7. Relative changes in (%) of micro- and macrophysical cloud properties in experiment *B* compared to experiment *NS* (derived from $\frac{B-NS}{NS} \cdot 100$): cloud droplet number concentration (CDNC) at cloud top (top left), CDNC concentrations (top right), cloud droplet effective radius (r_{eff}) at cloud top (bottom left) and cloud liquid water path (LWP) (bottom right). The black contour lines enclose areas showing statistical significance at the 90 % level.

ACPD
12, 7073–7123, 2012

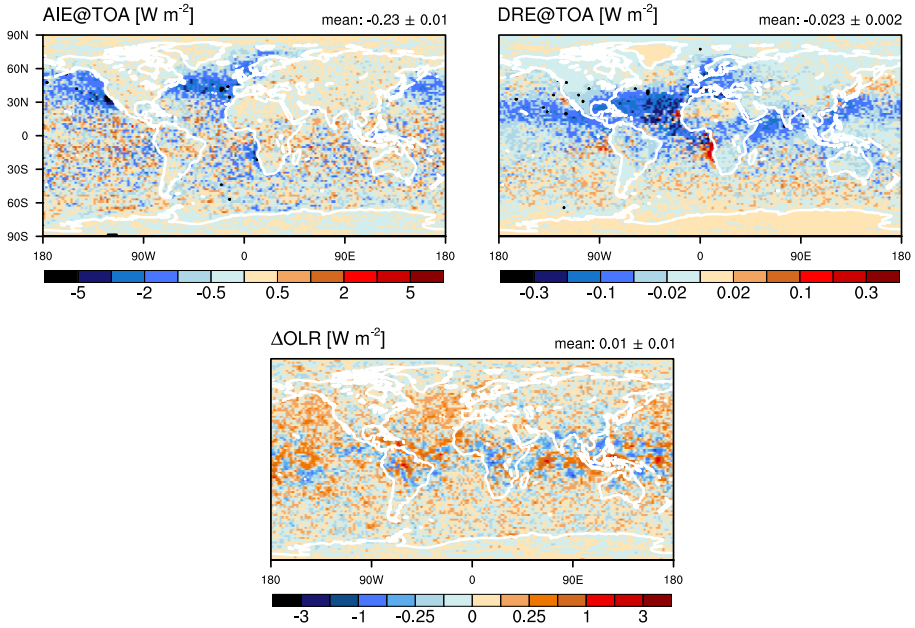

Fig. 8. Changes in top-of-atmosphere (TOA) radiation in experiment *B* with respect to experiment *NS*. The aerosol indirect effect (AIE, top left) is computed as the change in "net all-sky radiation – direct aerosol radiative perturbation", the direct radiative effect (DRE, top right) is the change in net clear-sky radiation and the change in outgoing longwave radiation (OLR, bottom) represents changes in net all-sky thermal radiation. The black contour lines enclose areas showing statistical significance at the 90 % level.

ACPD
12, 7073–7123, 2012

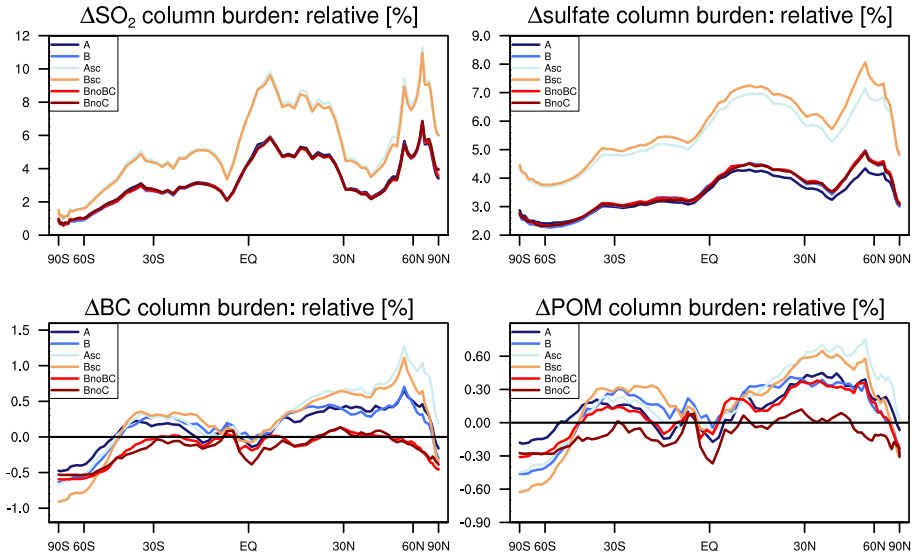

Fig. 9. Zonally averaged relative changes of atmospheric column burdens with respect to *NS* computed as $\left(\frac{\text{"experiment"}-NS}{NS}\cdot 100\right)$: sulphur dioxide ($SO_2$, top left), sulfate (top right), black carbon (BC, bottom left) and particulate organic matter (POM, bottom right).

ACPD
12, 7073–7123, 2012

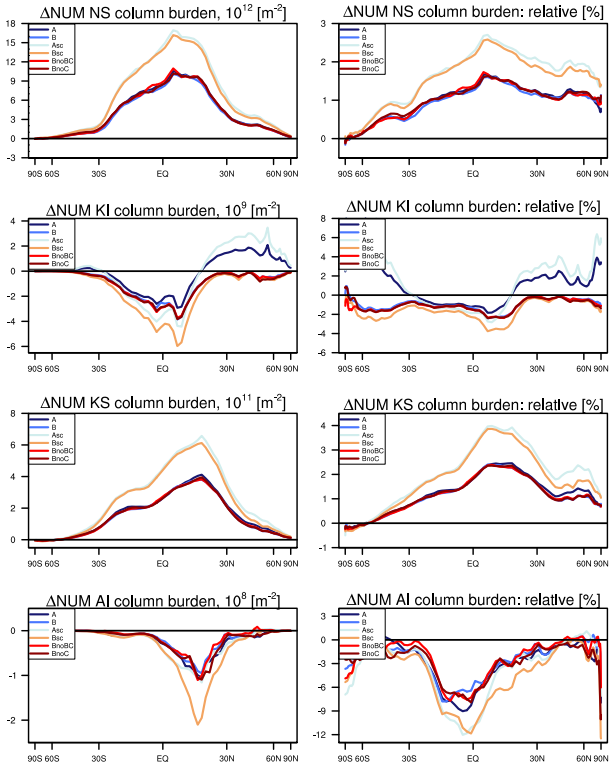

Fig. 10. Zonally averaged absolute- and relative changes of atmospheric column number burdens with respect to *NS* and aerosol mode in ECHAM-HAM: Nucleation mode soluble (*NS*, top), Aitken mode insoluble (KI, second from top), Aitken mode soluble (KS, second from bottom) and Accumulation mode insoluble (AI, bottom). Relative changes are derived from $\left(\frac{\text{"experiment"}-NS}{NS}\cdot 100\right)$.

ACPD
12, 7073–7123, 2012

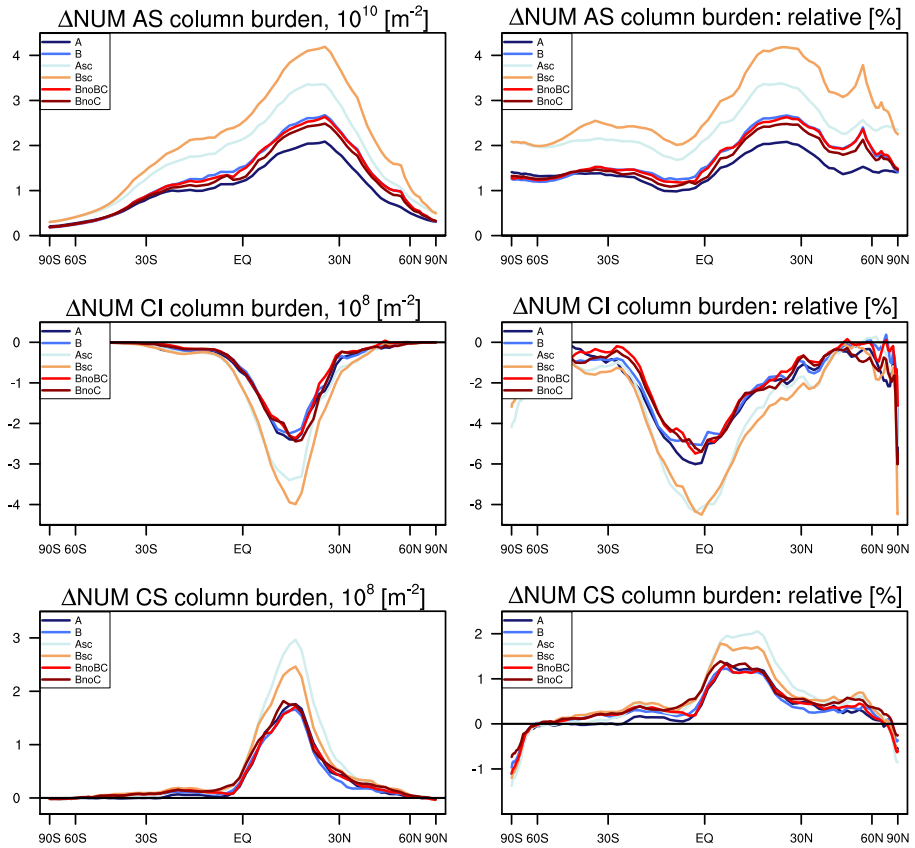

Fig. 11. Zonally averaged absolute- and relative changes of atmospheric column number burdens with respect to *NS* and aerosol mode in ECHAM-HAM: accumulation mode soluble (AS, top), Coarse mode insoluble (CI, middle) and Coarse mode soluble (CS, bottom). Relative changes are derived as $\left(\frac{\text{"experiment"}-NS}{NS}\cdot 100\right)$.

ACPD
12, 7073–7123, 2012

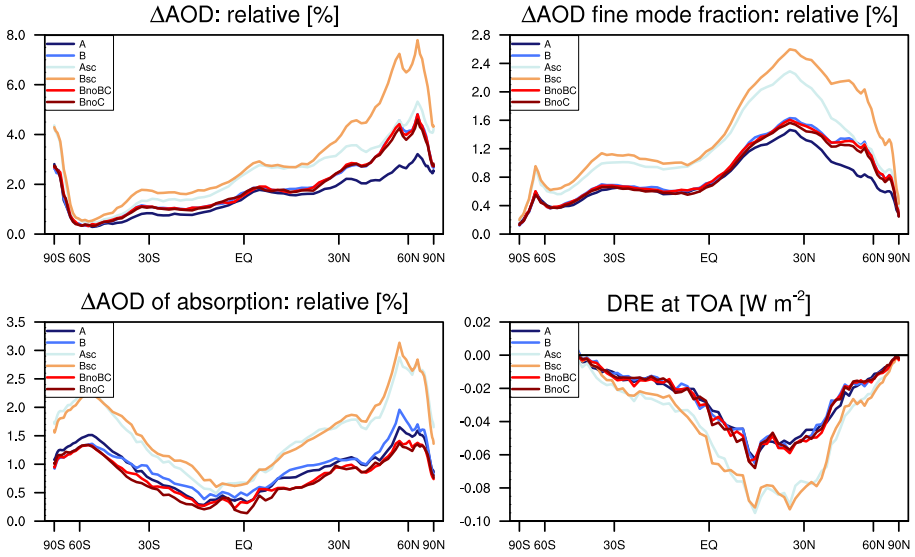

Fig. 12. Zonally averaged relative changes of quantities related to direct aerosol-radiation interaction with respect to *NS* computed as $\left(\frac{\text{"experiment"}-NS}{NS}\cdot 100\right)$: aerosol optical depth (AOD, top left), AOD fine mode (top right), AOD of absorption (bottom left). The resulting aerosol direct radiative effect (DRE) at TOA is also shown (bottom right).

ACPD
12, 7073–7123, 2012

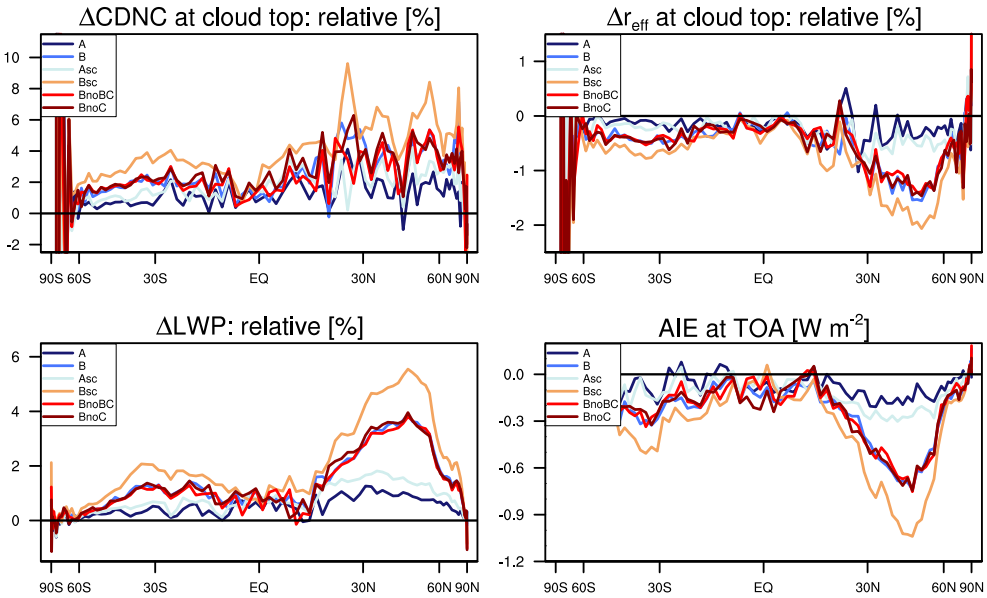

Fig. 13. Zonally averaged relative changes of quantities related to aerosol-cloud interaction with respect to *NS* computed as $\left(\frac{\text{"experiment"}-NS}{NS}\cdot 100\right)$: cloud droplet number concentration (CDNC) and cloud droplet effective radius (r_{eff}) at cloud top (top left and right) and cloud liquid water path (LWP, bottom left). The resulting AIE at TOA is also shown (bottom right).

ACPD
12, 7073–7123, 2012

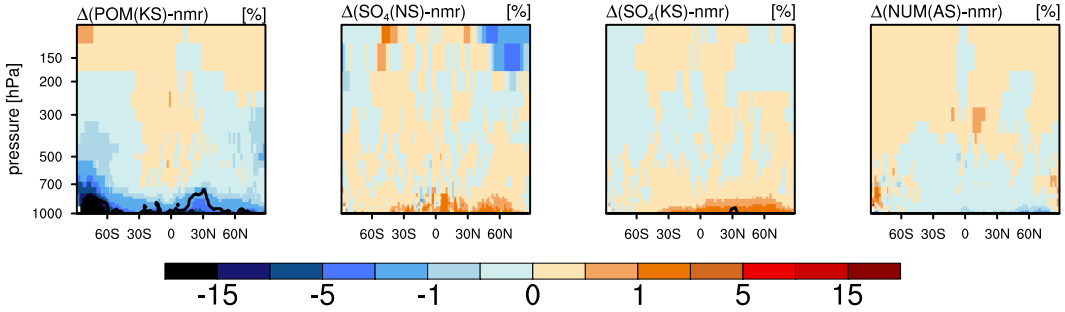

Fig. 14. Relative changes in (%) of temporally and zonally averaged changes in (from left to right) POM(KS), sulfate(NS and KS) mass mixing ratios and total number mixing ratio in AS in experiment *BnoC* compared to experiment *B* derived from $\left(\frac{BnoC-B}{B}\cdot 100\right)$. The black contour lines enclose areas showing statistical significance at the 90 % level.

ACPD
12, 7073–7123, 2012